

# RNDr. Thesis

Daniela eháková

2018

University of South Bohemia in České Budějovice  
Faculty of Science

# Genome stability of human induced pluripotent stem cells

RNDr. Thesis

Mgr. Daniela Čeháková

České Budějovice 2018

**Reháková, D. (2018): Genome stability of human induced pluripotent stem cells. RNDr. Thesis, 32 pp. Faculty of Science, University of South Bohemia, České Budějovice, Czech Republic**

Based on following original research articles:

**Simara, P., Tesarova, L., Rehakova, D., Matula, P., Stejskal, S., Hampl, A., & Koutna, I. (2017). DNA double-strand breaks in human induced pluripotent stem cell reprogramming and long-term in vitro culturing. *Stem cell research & therapy*, 8(1), 73.**

Annotation

Human induced pluripotent stem cells (hiPSCs) play roles in both disease modelling and regenerative medicine. It is critical that the genomic integrity of the cells remains intact and that the DNA repair systems are fully functional. In this article, we focused on the detection of DNA double-strand breaks (DSBs) by phosphorylated histone H2AX (known as  $\gamma$ -H2AX) and p53-binding protein 1 (53BP1) in three distinct lines of hiPSCs, their source cells, and one line of human embryonic stem cells (hESCs). We measured spontaneously occurring DSBs throughout the process of fibroblast reprogramming and during long-term in vitro culturing. To assess the variations in the functionality of the DNA repair system among the samples, the number of DSBs induced by  $\gamma$ -irradiation and the decrease over time was analysed. The foci number was detected by fluorescence microscopy separately for the G1 and S/G2 cell cycle phases. We demonstrated that fibroblasts contained a low number of non-replication-related DSBs, while this number increased after reprogramming into hiPSCs and then decreased again after long-term in vitro passaging. The artificial induction of DSBs revealed that the repair mechanisms function well in the source cells and hiPSCs at low passages but fail to recognize a substantial proportion of DSBs at high passages. Our observations suggest that cellular reprogramming increases the DSB number but that the repair mechanism functions well. However, after prolonged in vitro culturing of hiPSCs, the repair capacity decreases.

**Simara, P., Tesarova, L., Rehakova, D., Farkas, S., Salingova, B., Kutalkova, K., Vavreckova E., Matula P., Matula P., Veverkova L. & Koutna, I. (2018). Reprogramming of adult peripheral blood cells into human induced pluripotent stem cells as a safe and accessible source of endothelial cells. *Stem cells and development*, 27(1), 10-22.**

#### Annotation

New approaches in regenerative medicine and vasculogenesis have generated a demand for sufficient numbers of human endothelial cells (ECs). ECs and their progenitors reside on the interior surface of blood and lymphatic vessels or circulate in peripheral blood; however, their numbers are limited, and they are difficult to expand after isolation. Recent advances in human induced pluripotent stem cell (hiPSC) research have opened possible avenues to generate unlimited numbers of ECs from easily accessible cell sources, such as the peripheral blood. In this study, we reprogrammed peripheral blood mononuclear cells, human umbilical vein endothelial cells (HUVECs), and human saphenous vein endothelial cells (HSVECs) into hiPSCs and differentiated them into ECs. The phenotype profiles, functionality, and genome stability of all hiPSC-derived ECs were assessed and compared with HUVECs and HSVECs. hiPSC-derived ECs resembled their natural EC counterparts, as shown by the expression of the endothelial surface markers CD31 and CD144 and the results of the functional analysis. Higher expression of endothelial progenitor markers CD34 and kinase insert domain receptor (KDR) was measured in hiPSC-derived ECs. An analysis of phosphorylated histone H2AX (H2AX) foci revealed that an increased number of DNA double-strand breaks upon reprogramming into pluripotent cells. However, differentiation into ECs restored a normal number of H2AX foci. Our hiPSCs retained a normal karyotype, with the exception of the HSVEC-derived hiPSC line, which displayed mosaicism due to a gain of chromosome 1. Peripheral blood from adult donors is a suitable source for the unlimited production of patient-specific ECs through the hiPSC interstage. hiPSC-derived ECs are fully functional and comparable to natural ECs. The protocol is eligible for clinical applications in regenerative medicine if the genomic stability of the pluripotent cell stage is closely monitored.

## **Declaration [in Czech]**

Prohlašuji, že svoji rigorózní práci jsem vypracoval/a samostatně pouze s použitím pramenů a literatury uvedených v seznamu citované literatury. Prohlašuji, že v souladu s § 47b zákona č. 111/1998 Sb. v platném znění souhlasím se zveřejněním své rigorózní práce, a to v nezkrácené podobě elektronickou cestou ve veřejně přístupné části databáze STAG provozované Jihočeskou univerzitou v Českých Budějovicích na jejích internetových stránkách, a to se zachováním mého autorského práva k odevzdanému textu této kvalifikační práce. Souhlasím dále s tím, aby toutéž elektronickou cestou byly v souladu s uvedeným ustanovením zákona č. 111/1998 Sb. zveřejněny posudky kolektivu a oponentů práce i záznam o průběhu a výsledku obhajoby kvalifikační práce. Rovněž souhlasím s porovnáním textu mé kvalifikační práce s databází kvalifikačních prací Theses.cz provozovanou Národním registrem vysokoškolských kvalifikačních prací a systémem na odhalování plagiátů.

V Brně 30.4.2018

Daniela Šeháková

## **P** iznání spoluautorství [in Czech]

Svým podpisem potvrzují významné spoluautorství Mgr. Daniely Šehákové na následujících publikacích:

**DNA double-strand breaks in human induced pluripotent stem cell reprogramming and long-term in vitro culturing**, Stem Cell Research & Therapy, 2017 (IF=4,21)

**Reprogramming of Adult Peripheral Blood Cells into Human Induced Pluripotent Stem Cells as a Safe and Accessible Source of Endothelial Cells**, Stem Cells and Development, 2018 (IF=3,56).

Mgr. Daniela Šeháková v rámci těchto publikací udržovala buněčné kultury, připravovala vzorky, vyhodnocovala data a podílela se na úpravách textu.

Konkrétně se jednalo o práci především s lidskými indukovanými pluripotentními kmenovými buňkami, případně jinými lidskými buněčnými kulturami, včetně sledování základních vlastností těchto buněčných linií (případně pomocí PCR a flow-cytometrie). Buněčné kultury zpracovávala pro imunocytochemické barvení, snímala pomocí mikroskopu Zeiss a následně prováděla analýzu obrazu a statistické zpracování a podílela se na vyhodnocení takto získaných dat.

Mgr. Pavel Třmára, Ph.D.

## **Author's note**

Human induced pluripotent stem cells (hiPSCs) can be induced from tissues of an adult and they can be differentiated into chosen cell type which gives many possibilities for their use in both research and medicine.

Stem cells are defined by their abilities to self-renew and differentiate. Depending on the environment they can divide either to cells of the same cell type as the mother cell, or to more differentiated cells. Stem cells are natural component of the organism, they are present both during the development and in an adult individual. In an organism, most of these cells is quiescent.

Stem cells in vitro are however kept in an environment that forces them to grow and divide constantly. That allows us to grow large quantity of cells, but it comes with a risk of genome instability, as cells during the short cell cycle have little time to check for possible damage and to repair it. That is why monitoring DNA damage is of importance.

In presented studies, DNA damage and response to it was studied via phosphorylated histone H2AX ( H2AX). This phosphorylation is an early cellular response to DNA damage, specifically, double strand breaks (DSBs). After immunocytochemical staining, it can be observed as foci in nucleus, which were counted using image analysis. As these foci can be formed as a response to replication stress, cells in S or G2 phase of cell cycle were marked with EdU and only cells in G1 phase were analyzed.


Two papers on this subject are presented. The first study focuses on evaluating DNA damage in hiPSCs during prolonged culture and the second is comparing DNA damage of source cells, hiPSCs and hiPSCs-derived epithelial cells.

RESEARCH

Open Access



# DNA double-strand breaks in human induced pluripotent stem cell reprogramming and long-term in vitro culturing

Pavel Simara<sup>1\*</sup> , Lenka Tesarova<sup>1</sup>, Daniela Rehakova<sup>1</sup>, Pavel Matula<sup>1</sup>, Stanislav Stejskal<sup>1</sup>, Ales Hampl<sup>2</sup> and Irena Koutna<sup>1</sup>

## Abstract

**Background:** Human induced pluripotent stem cells (hiPSCs) play roles in both disease modelling and regenerative medicine. It is critical that the genomic integrity of the cells remains intact and that the DNA repair systems are fully functional. In this article, we focused on the detection of DNA double-strand breaks (DSBs) by phosphorylated histone H2AX (known as  $\gamma$ H2AX) and p53-binding protein 1 (53BP1) in three distinct lines of hiPSCs, their source cells, and one line of human embryonic stem cells (hESCs).

**Methods:** We measured spontaneously occurring DSBs throughout the process of fibroblast reprogramming and during long-term in vitro culturing. To assess the variations in the functionality of the DNA repair system among the samples, the number of DSBs induced by  $\gamma$ -irradiation and the decrease over time was analysed. The foci number was detected by fluorescence microscopy separately for the G1 and S/G2 cell cycle phases.

**Results:** We demonstrated that fibroblasts contained a low number of non-replication-related DSBs, while this number increased after reprogramming into hiPSCs and then decreased again after long-term in vitro passaging. The artificial induction of DSBs revealed that the repair mechanisms function well in the source cells and hiPSCs at low passages, but fail to recognize a substantial proportion of DSBs at high passages.

**Conclusions:** Our observations suggest that cellular reprogramming increases the DSB number but that the repair mechanism functions well. However, after prolonged in vitro culturing of hiPSCs, the repair capacity decreases.

**Keywords:** Human induced pluripotent stem cells, DNA double-strand breaks,  $\gamma$ H2AX, 53BP1, Long-term in vitro culture, DNA repair

## Background

Human induced pluripotent stem cells (hiPSCs) hold great promise for clinical applications because of their potential to differentiate into all three embryonic germ layers [1–3]. To use hiPSCs in cell therapy or disease modelling [4], it is fundamental that they possess an intact genome. Much research has been performed in the field of genome maintenance in mouse and human embryonic stem cells (hESCs). However, less is known

about the causes of genomic aberrations and the functionality of repair mechanisms in hiPSCs [5]. In general, the genomic instabilities in hiPSCs may be introduced: 1) by pre-existing mutations in source cells; 2) during reprogramming; and 3) during in vitro expansion of the hiPSCs. It has been reported that at least 50% of the single-nucleotide variations in hiPSCs pre-existed in the source cells [6]. The process of reprogramming itself represents a serious risk of mutation acquisition. Primarily, deletions of tumour suppressor genes were observed during reprogramming [7]. Using episomal vectors may lower the risk of reprogramming-associated genome changes [8]. The culturing of pluripotent stem cells (PSCs) in vitro

\* Correspondence: p.simara@mail.muni.cz

<sup>1</sup>Centre for Biomedical Image Analysis, Faculty of Informatics, Masaryk University, Kamenice 5, 625 00 Brno, Czech Republic

Full list of author information is available at the end of the article





is probably the main cause of the accumulation of genomic instabilities, resulting from the adaptation to culture conditions and clonal selection during passaging. The data reported by Taapken et al. [9] support this idea, indicating that the types and frequency of karyotypic abnormalities are similar between hESCs and hiPSCs. In contrast, the results of Laurent et al. [7] revealed slight differences in the distribution of sub-chromosomal variations between hESCs and hiPSCs. Interestingly, in their study [7], prolonged in vitro culturing was associated with oncogene duplication.

One of the key techniques for monitoring DNA integrity is the detection of DNA double-strand breaks (DSBs). DSBs are a severe type of DNA damage that may cause irreversible changes in the genomic content of the cell. They are induced by internal factors such as the by-products of cell metabolism or replication stress, or by external factors such as exposure to irradiation or chemical agents [10]. A damaged cell may arrest the cell cycle until the lesions are repaired. If the DNA damage is not successfully repaired, apoptosis is commonly induced to prevent the propagation of chromosomal aberrations. The repair of DSBs is executed either by fast non-homologous end-joining (NHEJ) or more precise homologous recombination (HR). Both mechanisms contribute to DSB repair in a cell cycle-specific manner. NHEJ occurs at all phases of the cell cycle but is primarily responsible for DSB repair in the G1 stage. HR occurs predominantly in the late S and G2 phases [11]. Published data suggest that pluripotent cells exert stronger genomic protection and can repair DNA lesions more efficiently than differentiated somatic cells [5, 12–14]. However, a strong DNA protective mechanism may cause the pluripotent cells to be more prone to apoptosis.

Various DNA damage-response proteins have been used as markers of DSBs, including phosphorylated histone H2AX (known as  $\gamma$ H2AX) and p53-binding protein 1 (53BP1) [15]. The generation of  $\gamma$ H2AX foci at the site of DNA lesions precedes the formation of 53BP1 foci [16–18]. Several studies have confirmed that 53BP1 functions exclusively in NHEJ and that it inhibits the 5' end resection needed for HR [19–21]. In contrast,  $\gamma$ H2AX influences both NHEJ and HR [10]. The foci formation of  $\gamma$ H2AX is dependent on the cell cycle phase [22–24]. S/G2 phase cells exhibit more  $\gamma$ H2AX foci than do cells in G1 phase because of replication-related DSBs. Cell-cycle dependency has not been observed for 53BP1 [25].

In the present study, we compared the genomic integrity of fibroblasts and pluripotent stem cells. We used fluorescence microscopy to visualize the DSBs recognized by  $\gamma$ H2AX and 53BP1 in three hiPSC lines and one hESC line at low or high passage numbers and in

one line of source cell fibroblasts. Each hiPSC line is unique and represents a different reprogramming approach, as described in the Methods. We also aimed to detect differences in the ability to recognize DSBs artificially induced by  $\gamma$ -irradiation and their decrease over time. The measurements were conducted with respect to cell cycle stage, and the data were analysed separately for the G1 and G2/S phases. Thus, we aimed to elucidate genomic stability during hiPSC generation and in vitro culturing.

## Methods

### hiPSC generation and cell culture

Human dermal fibroblasts (hDFs; kindly provided by the National Tissue Centre Inc., Brno, Czech Republic) and CD34<sup>+</sup> haematopoietic progenitors (blood sample kindly provided by the Department of Internal Medicine, Haematology and Oncology, Masaryk University, and University Hospital Brno, Czech Republic) were used as source cells for the generation of hiPSCs as described in Šimara et al., 2014 [26, 27]. For this study, we used the hiPSC line CBIA-3–CD34<sup>+</sup> haematopoietic progenitors reprogrammed by the Sendai virus (CytoTune™-iPS Reprogramming Kit; Thermo Fisher Scientific, Waltham, MA, USA), hiPSC line CBIA-5–fibroblasts reprogrammed by the Sendai virus, and hiPSC line CBIA-7–fibroblasts reprogrammed by episomal vectors (Epi5™ Episomal iPS Reprogramming Kit; Thermo Fisher Scientific). The CCTL-14 hESC line [28] was a kind gift from the Department of Histology and Embryology (Faculty of Medicine, Masaryk University, Brno, Czech Republic). All three hiPSC lines and the hESC line were maintained in the form of colonies on irradiated mouse embryonic fibroblast feeder cells (MEFs;  $2.5 \times 10^5$  cells per 3.5-cm dish) in DMEM/F12 (1:1) supplemented with 20% knock-out serum replacement, 2 mM L-glutamine, 100  $\mu$ M non-essential amino acids, 1% penicillin/streptomycin, 0.1 mM 2-mercaptoethanol, and 10 ng/ml basic fibroblast growth factor (bFGF) (all from Thermo Fisher Scientific). The medium was changed daily. Markers of pluripotency (Oct-3/4, Sox2, Nanog, and SSEA4) were detected as described previously [26], and all three hiPSC lines were positive for all of these markers (Additional file 1: Figure S1). A teratoma formation assay confirmed that the hiPSCs could differentiate into all three germ layers (Additional file 2: Figure S2).

The following cell passage numbers (p) were used (low and high): CBIA-3 at p27 and p76, CBIA-5 at p19 and p65, CBIA-7 at p25 and p67, and CCTL-14 at p30 and p302. hDFs were used at p6. No CD34<sup>+</sup> blood progenitors used to generate CBIA-3 were available for DSB analysis.

### **$\gamma$ -Irradiation**

Prior to irradiation, the hiPSCs and hESCs were feeder depleted by culturing on a Geltrex<sup>®</sup> matrix for 3 days. Essential 8<sup>™</sup> medium (Thermo Fisher Scientific) was changed daily. The cells were then irradiated by ionizing radiation (IR; 0.5 Gy/min; <sup>137</sup>Cs; 1 and 4 Gy) to induce DSBs and fixed in 4% paraformaldehyde at 0.5, 2, and 6 h after irradiation.

The dose of 1 Gy was selected for the experiments based on published results [12, 29] and our DSB count measurement after 1 Gy or 4 Gy irradiation (data not shown). The peak value of the foci number was recorded 0.5 h after irradiation; therefore, this time point was selected for the study of the functionality of the repair system.

### **Immunocytochemistry**

Immunocytochemical staining was used to visualize the DSBs and distinguish between the cell cycle stages G1 and S/G2. Four hours before fixation, a nucleoside analogue of thymidine, 5-ethynyl-2'-deoxyuridine (EdU; Thermo Fisher Scientific), was added at a final concentration of 10  $\mu$ M. The cells were fixed in 4% paraformaldehyde and permeabilized in 0.2% Triton-X (both from Sigma-Aldrich, St. Louis, MO, USA). Overnight incubation with primary antibodies against  $\gamma$ H2AX (Biolegend, San Diego, CA, USA) and 53BP1 (Santa Cruz Biotechnology, Dallas, TX, USA) was followed by 1 h of incubation with a secondary antibody conjugated with Alexa 555 (Cell Signaling Technology, Danvers, MA, USA). The samples were stained with the Click-iT<sup>®</sup> EdU Alexa Fluor<sup>®</sup> 488 Imaging Kit (Thermo Fisher Scientific) to visualize EdU according to the manufacturer's instructions. Finally, the nuclei were stained with Hoechst dye (BisBenzemide H33342; 1  $\mu$ g/ml; Sigma-Aldrich).

### **Fluorescence microscopy and image analysis**

Fluorescent signals were detected using the Zeiss Axiovert 200 M system (Carl Zeiss, Oberkochen, Germany). The images were captured using a CoolSNAP HQ2 CCD camera in the wide-field mode (Photometrics, Tucson, AZ) at  $-30$  °C. Thirty 3- $\mu$ m slices were acquired in each field at a resolution of  $1392 \times 1040$  pixels. The pixel size of the images was  $124 \times 124$  nm. Between 500 and 1000 cells were analysed from each microscopic slide. Two slides,  $\gamma$ H2AX and 53BP1, were prepared from each sample and each time point.

Acquarium software, developed by our group, was used to acquire and analyse the images [30]. Aquarium is open source software available for download at our group's official website (<http://cbia.fi.muni.cz/projects/acquarium.html>). During the analysis, individual cells in the field of view were first cropped manually. Next, the nucleus of each cell, stained with Hoechst dye, was

recognized automatically using the "Find objects (hysteresis thresholding)" plugin. We used the Gaussian filter in the preprocessing phase (with  $\sigma = 1$ ), the threshold was calculated using the two-level Otsu method, and we defined the minimum size of an object to exclude the parts of adjacent cells. This plugin defined the area in which we counted  $\gamma$ H2AX or 53BP1 foci. For this purpose, we employed the eMax algorithm described in [31] using the parameters  $\sigma = 1$ , a spot height threshold of 80, and a maximum spot size of 800, which we set empirically. The EdU signal was quantified based on the total intensity calculated in the nucleus. The threshold for the separation of EdU-negative (G1) and EdU-positive (S/G2) cells was computed in MATLAB (Mathworks) using the Otsu method.

### **Flow cytometry analysis**

To assess early apoptosis, cells were stained with Annexin-V fluorescein isothiocyanate (FITC) and 7-amino-actinomycin D (7-AAD; BD Via-Probe) in Annexin-V binding buffer (Miltenyi Biotec, Bergisch Gladbach, Germany). From each sample, approximately  $1 \times 10^5$  cells were processed. All of the samples were measured using a BD FACS Canto II flow cytometer (Becton-Dickinson). BD FACSDiva (Becton-Dickinson) software was used for the data analysis.

### **Western blotting**

For each time point, approximately  $1 \times 10^6$  cells were lysed in RIPA buffer. The total protein concentration was assessed using a Pierce<sup>™</sup> BCA Protein Assay Kit (Thermo Fisher Scientific). Laemmli buffer was added, and the samples were separated by SDS-PAGE. The proteins were transferred onto polyvinylidene fluoride membranes, and the membranes were blocked with 5% milk in TBS-Tween for 1 h. The membranes were then incubated with a 1:1000 dilution of PARP and GAPDH primary antibodies (both from Cell Signaling Technology) in TBS-Tween with 5% milk at 4 °C overnight. Subsequently, the membranes were incubated with the secondary antibody (1:5000 anti-rabbit HRP; Cell Signaling Technology) for 1 h at room temperature, and the blots were developed using the Clarity<sup>™</sup> Western ECL Substrate (Bio-Rad Laboratories, Hercules, CA, USA) according to the manufacturer's instructions.

### **Statistical analysis**

Comparison of two data sets was performed using Student's *t* test. Multi-group assays were analysed by a one-way analysis of variance (ANOVA) in conjunction with Tukey's test. A level of  $P < 0.05$  was considered to be statistically significant.

## Results

### Discrimination between the cell cycle phases using EdU increases the accuracy of analysing DNA lesions

The overall goal of our study was to use the numbers of  $\gamma$ H2AX and 53BP1 foci as a measure of DNA repair in hiPSCs and in their somatic founders. However, as described above, it has been previously shown that the numbers of  $\gamma$ H2AX foci are influenced by the cell cycle phase, with more foci being present in the S/G2 nuclei than in the G1 nuclei [22–24]. Obviously, different types of cells (somatic versus pluripotent) as well as cells in different states of culture (early versus late) most likely differ in the lengths of the individual phases of their cell cycle. Therefore, we first determined to what extent the numbers of foci are influenced by cell cycle speed and may thus distort the overall picture obtained by the foci analysis. To do so, we labelled newly synthesized DNA with EdU, visualized the accumulation of  $\gamma$ H2AX and 53BP1 proteins on chromatin (foci), and then used an automated analysis. This approach is shown in Fig. 1a. Figure 1b and c exemplify the situation when an EdU-positive cell (nucleus) contains a larger number of  $\gamma$ H2AX foci compared to EdU-negative cells (nuclei). Before we counted the numbers of  $\gamma$ H2AX and 53BP1 foci, we analysed the EdU signal distribution among the cell samples and separated the EdU-negative (G1 phase) and EdU-positive (S/G2 phase)

nuclei. The EdU signal strength in particular cells in each sample was then expressed as a histogram (with a calculated threshold for EdU negativity) for maximum clarity and reproducibility in separating G1 and S/G2 cells. Histograms of all analysed samples are shown in Additional file 3 (Figure S3). Our data revealed a statistically significant difference in cell cycle phase distribution between hDFs, representing a somatic cell type, and all pluripotent stem cells, irrespective of their type and passage number (Fig. 2). The high proportion (87.2%) of EdU-negative cells in the hDF sample suggests that the vast majority of these cells remain in G1 phase. By contrast, only between 49.5 and 57.0% of the pluripotent cells were EdU negative, confirming their high proliferation activity and short cell cycle.

Taken together, this series of experiments demonstrates the robustness of the approach that we have developed to visually discriminate between G1 and S/G2 cells in situ. Our data show that, using this technique, we can identify changes in cell cycle progression. In the context of cell cycle-associated differences in numbers of  $\gamma$ H2AX and 53BP1 foci, this approach is extremely useful and was employed for all the following analyses in this study. The Acquiarius software also represents an extremely valuable tool for complex and automated microscope image analysis.

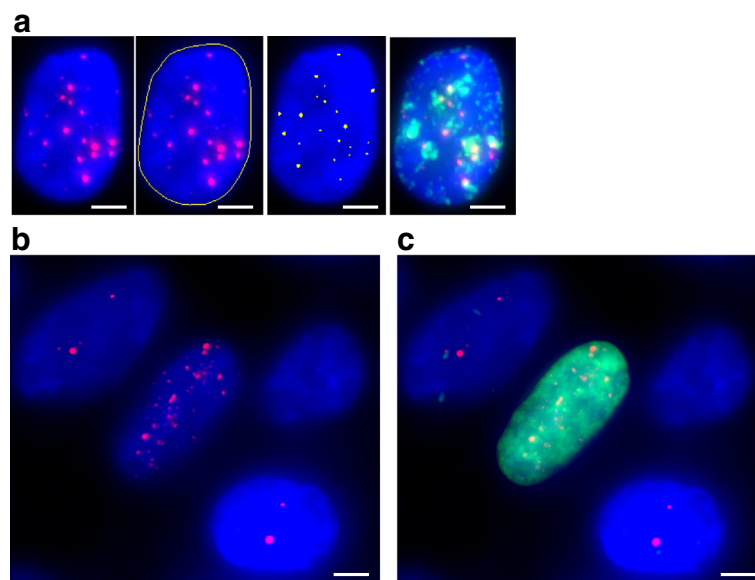


**Fig. 1** Image analysis in three dimensions using Acquiarius software. **a** Automatic detection of the cell nucleus (blue) marked with a yellow border line and counting of 21  $\gamma$ H2AX foci (red) inside the cell nucleus, visualized by yellow dots. The green regions emerge as EdU is newly incorporated during DNA synthesis. **b** A significantly higher count of  $\gamma$ H2AX foci is seen in the nucleus of the cell in the middle of the field than in the adjacent cells. **c** The cell in the middle is strongly positive for EdU (green), suggesting that the cell passes through the S or G2 phase, and  $\gamma$ H2AX foci result from replication stress. The hiPSC line CBIA-5 at low passage, non-irradiated control,  $\gamma$ H2AX. A merge of 30 3- $\mu$ m slices is shown. Scale bar = 5  $\mu$ m. EdU 5-ethynyl-2'-deoxyuridine

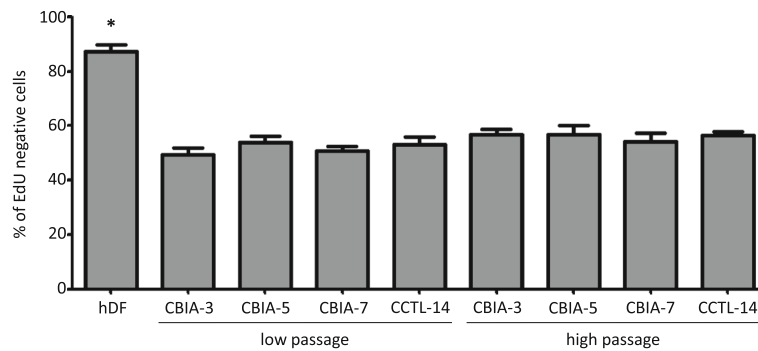


**Fig. 2** Distribution of EdU-negative cells in the samples. Comparison of fibroblasts (hDF), hiPSCs (CBI A-3, CBI A-5, and CBI A-7), and hESCs (CCTL-14) at low or high passage number. The mean value of the percentage of EdU-negative cells calculated from six histograms is shown ( $\pm$  SEM). A massive disproportion in the EdU-negative cell group was observed between hDF somatic cells and pluripotent stem cells. \* $P < 0.05$  by one-way ANOVA and Tukey's multiple comparison test. *EdU* 5-ethynyl-2'-deoxyuridine, *hDF* human dermal fibroblast

**Reprogramming is accompanied by increased numbers of  $\gamma$ H2AX and 53BP1 foci, but this trend is reversed with prolonged in vitro culturing**

First, we wanted to determine whether reprogramming to pluripotency influences the numbers of DSBs as revealed by the presence of  $\gamma$ H2AX and 53BP1 foci. To do so, we counted these foci in the parent fibroblasts (hDFs) and in cells of three independent hiPSC lines (CBI A-3, CBI A-5,

and CBI A-7) at an early stage after their establishment (up to passage 27; further referred to as low-passage hiPSCs). As shown in Fig. 3a and b, the numbers of both types of foci in EdU-negative hiPSCs were higher than those observed in EdU-negative hDFs. Specifically, in hDFs, the average number of foci per cell was only 1.1 for  $\gamma$ H2AX and 1.5 for 53BP1. In hiPSCs, however, these numbers ranged from 5.6 to 5.9 for  $\gamma$ H2AX and from 2.1 to 4.0

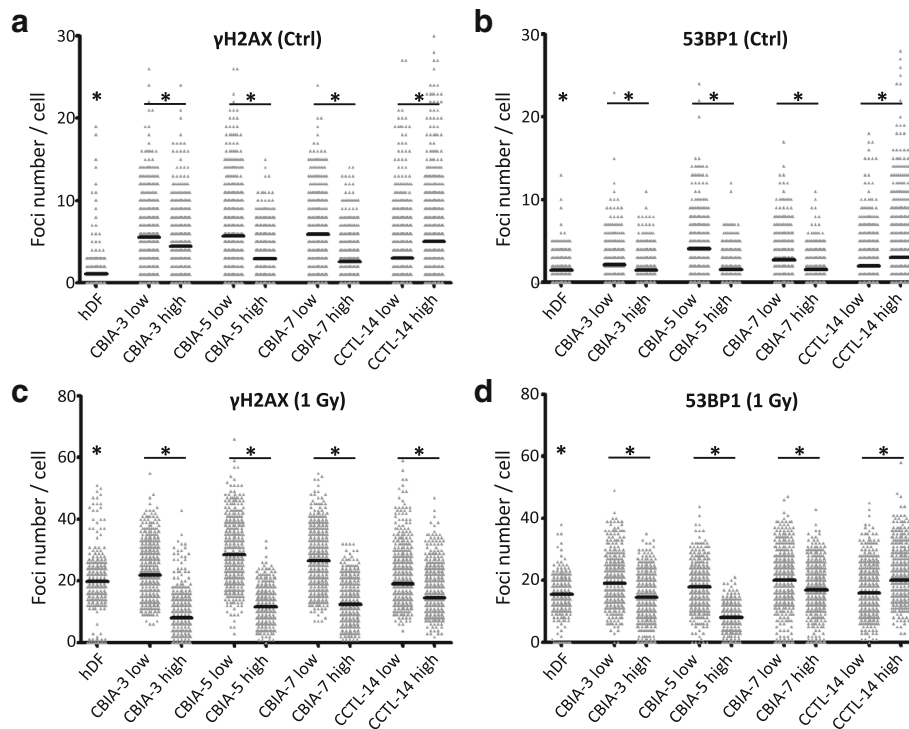


**Fig. 3** DSBs recognized by  $\gamma$ H2AX (a,c) and p53-binding protein 1 (53BP1) (b,d) in non-irradiated control cells (Ctrl) (a,b) or 0.5 h after  $\gamma$ -irradiation with 1 Gy (c,d). Comparison of fibroblasts (human dermal fibroblast; *hDF*), hiPSCs (CBI A-3, CBI A-5, and CBI A-7) and hESCs (CCTL-14) at low or high passage number. The number of foci in each cell is visualized as a dot, and the mean value is shown as a black line for each sample. The results are shown in the EdU-negative population. \* $P < 0.05$  between hDF and iPSCs in low passage, and between low and high passages, by one-way ANOVA and Tukey's multiple comparison test



for 53BP1. It needs to be stressed that the CBIA-5 and CBIA-7 cells produced about the same numbers of  $\gamma$ H2AX foci (5.69 and 5.89, respectively) despite the different reprogramming method used to generate these cells (Sendai virus versus episomal vectors). The next question was whether prolonged passaging of hiPSCs may further affect the number of DSBs. To obtain this information, we evaluated foci in hiPSCs (all three lines as above) that were cultured for a minimum of 65 passages (further referred to as high-passage cells). In these high-passage hiPSCs, the numbers of foci decreased (compared to low-passage cells), reaching levels of only 2.6 to 4.4 foci per cell for  $\gamma$ H2AX and 1.5 to 1.6 foci per cell for 53BP1.

As described in the previous section, EdU-positive (S/G2) cells are characterized by many more DSBs than EdU-negative (G1 phase) cells, possibly as a result of replicative stress-associated amplification of DNA lesions during the progression of the cell cycle. Accordingly, the numbers of both  $\gamma$ H2AX and 53BP1 foci were increased in EdU-positive cells compared to EdU-negative cells in all cell lines and passage categories (low and high) analysed in this experiment (Fig. 4). Interestingly, this S/G2-linked increase was the highest in hDFs, with the mean numbers of foci per EdU-positive cell being 29.9 for  $\gamma$ H2AX and 19.6 for 53BP1, probably reflecting their highly effective “healthy” repair machinery. In the low-passage hiPSCs, the respective mean numbers were slightly lower than in hDFs, 23.0–25.1 for  $\gamma$ H2AX and 8.8–15.3 for 53BP1, while in high-passage hiPSCs these numbers dropped down to 11.0–17.9 for  $\gamma$ H2AX and 4.7–6.5 for 53BP1. It is also of note that the mean numbers of  $\gamma$ H2AX foci were always (in all cell lines as well as passage categories) higher than those of 53BP1 foci (Fig. 4a).

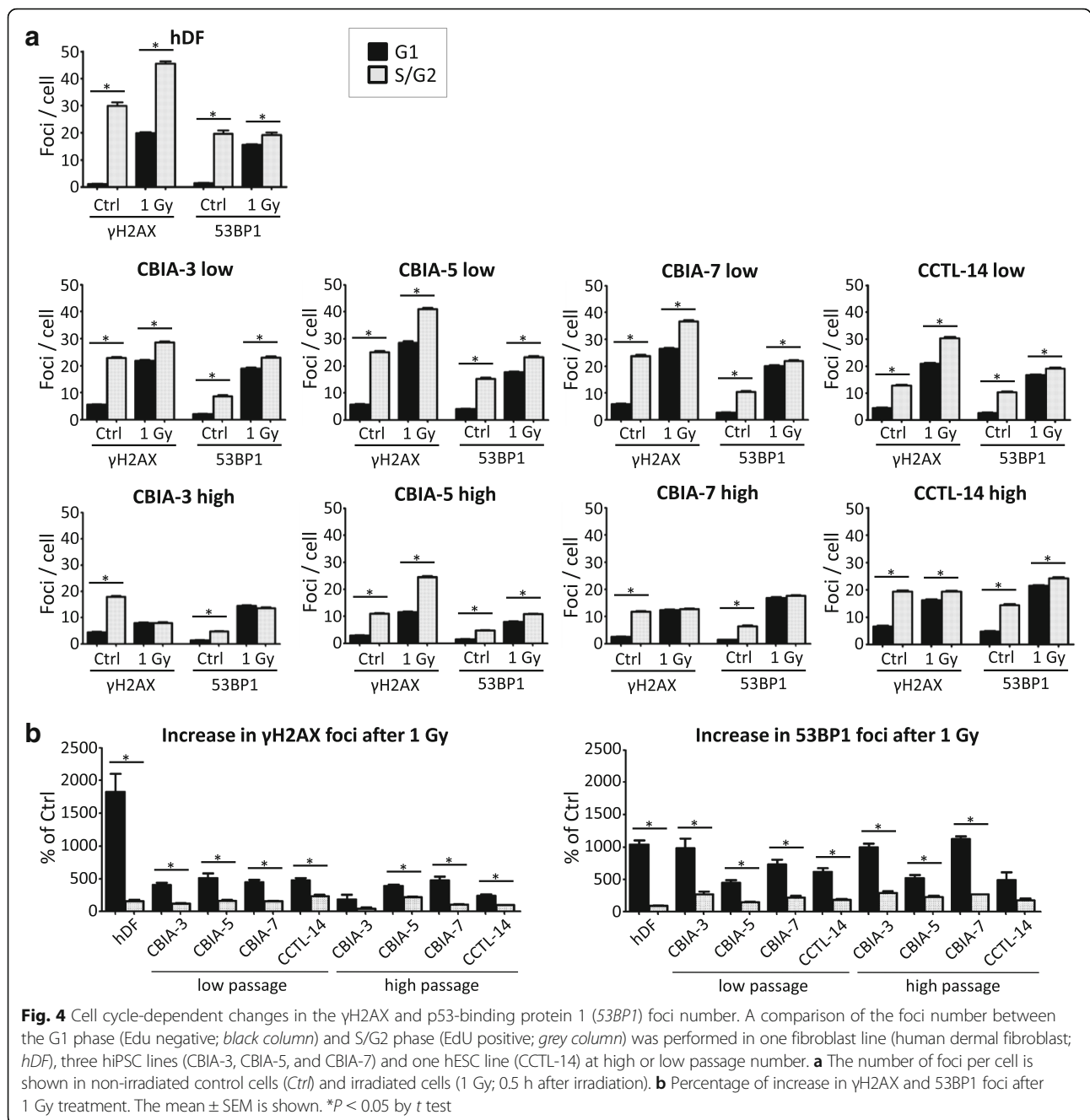
Since we hypothesized that increased DSBs are due to reprogramming rather than being associated with pluripotency, we thought that hESCs would have a rather low basal level of DSBs, possibly about the same as in hDFs. To address this issue, we also analysed a reference line of hESCs (CCTL-14) that we have shown in our previous work to conform in all aspects to hESC standards [28]. Contrary to our expectation, the numbers of DSB-associated foci in new, low-passage hESCs were much closer to those in hiPSCs than in hDFs. This held true for both EdU-negative and EdU-positive cells. Specifically, in EdU-negative cells the numbers averaged 4.5 for  $\gamma$ H2AX and 2.7 for 53BP1 foci, and in EdU-positive cells they averaged 12.8 for  $\gamma$ H2AX and 10.3 for 53BP1 foci. Clearly, the numbers of foci in hESCs follow the same trend as in hDFs and hiPSCs, being dramatically increased in S/G2 cells compared to the cells in G1 phase. Additionally, as in hDFs and hiPSCs, the numbers of  $\gamma$ H2AX foci in hESCs were always higher than those of

53BP1 foci. Surprisingly, however, in hESCs the numbers of  $\gamma$ H2AX- and 53BP1-associated foci further increased with their prolonged culturing, which was in strict contrast to what we observed in hiPSCs (see above). Specifically, the numbers of foci per cell in high-passage hESCs were as follows: in the EdU-negative cells, 6.7 for  $\gamma$ H2AX and 4.8 for 53BP1 foci; in the EdU-positive cells, 19.3 for  $\gamma$ H2AX and 14.3 for 53BP1 foci. The complete set of foci numbers is shown in Table 1.

#### hiPSCs lose their DNA repair capacity after prolonged maintenance in vitro

The above experiments demonstrated that, under normal culture conditions, hDFs, hiPSCs, and hESCs all have characteristic numbers of  $\gamma$ H2AX and 53BP1 foci. However, based on these measurements we cannot resolve whether this is due to differences in the level of “spontaneous” DNA damage, DNA repair capability (recognition of DNA lesions), or both. It is understood that the amount of DSBs in cultured cells caused by  $\gamma$ -irradiation is about the same for the same dose of irradiation, regardless of the type of cell. With this holding true, the numbers of  $\gamma$ H2AX and 53BP1 foci detected in cells irradiated by the same dose of  $\gamma$ -rays should then reflect the capability of the DNA repair machinery to recognize DSBs rather than the level of DNA damage. In the following series of experiments, we built on this presumption to study the DNA repair efficiency of human pluripotent stem cells. We irradiated the respective cells (hDFs, hiPSCs, and hESCs) with the same dose of  $\gamma$ -rays (1 Gy) and then determined the number of  $\gamma$ H2AX and 53BP1 foci at three different time points after irradiation (0.5, 2, and 6 h). It has previously been shown that the levels of  $\gamma$ H2AX and 53BP1 loaded onto chromatin usually reach a maximum at approximately 15–30 min after ionizing irradiation [32–34]. Based on this data, we used 30 min as the starting point. Two additional time points (2 and 6 h) then provided information on how DNA repair is sustained.

Figure 3c and d show the numbers of  $\gamma$ H2AX and 53BP1 foci 30 min after  $\gamma$ -irradiation in EdU-negative cells. As expected for normal cells, hDFs exhibited a dramatic increase to 19.9 and 15.6, respectively. This represents an 18-fold (for  $\gamma$ H2AX) and 10-fold (for 53BP1) increase over their numbers in non-irradiated controls, which indeed mirrors a massive initiation of DNA repair pathways (Fig. 4b). Surprisingly, although the numbers of both types of foci were higher in non-irradiated hiPSCs (irrespective of their passage number) than in hDFs (see the previous section), this was not the case for irradiated hiPSCs. Specifically, at 30 min after irradiation, low-passage hiPSCs produced 21.9 to 28.6  $\gamma$ H2AX foci and 17.8 to 20.1 53BP1 foci, thus always



exceeding the corresponding numbers observed in hDFs. In contrast, high-passage hiPSCs produced only 8.0 to 12.4 γH2AX foci and 8.0 to 16.9 53BP1 foci. In other words, in hiPSCs, their prolonged passaging dramatically diminished the numbers γH2AX and 53BP1 foci induced by γ-rays to levels below or similar to those observed in hDFs.

As described in the previous section, the numbers of “spontaneous” γH2AX and 53BP1 foci were, for all cell types and categories studied here, always higher in S/G2 (EdU-positive) than in G1 (EdU-negative) cells. In hiPSCs,

the fold-increase ranged from three-times in high-passage CBIA-5 cells (53BP1) to 4.6-times in high-passage CBIA-7 cells (γH2AX), and the changes were consistently statistically significant (Fig. 4a). This overall trend was also retained in γ-irradiated cells (at 30 min after irradiation); however, the actual fold-increase (S/G2 versus G1) was much lower, in four cases showing either no changes or statistically insignificant changes (for both γH2AX and 53BP1 foci in high-passage CBIA-3 and CBIA-7 hiPSCs) (Fig. 4a). Specifically, for hiPSCs, the fold-increase ranged from none to 2.1-times (24.6/11.6) for γH2AX foci in

**Table 1** Number of foci per cell

	Non-irradiated control cells				Irradiated cells (1Gy)			
	G1 (EdU-negative cells)		S/G2 (EdU-positive cells)		G1 (EdU-negative cells)		S/G2 (EdU-positive cells)	
	No. of foci $\pm$ SEM	No. of cells	No. of foci $\pm$ SEM	No. of cells	No. of foci $\pm$ SEM	No. of cells	No. of foci $\pm$ SEM	No. of cells
hDF								
$\gamma$ H2AX	1.13 $\pm$ 0.11	463	29.9 $\pm$ 1.32	60	19.89 $\pm$ 0.36	485	45.49 $\pm$ 0.88	97
53BP1	1.49 $\pm$ 0.07	486	19.64 $\pm$ 1.23	80	15.55 $\pm$ 0.22	501	19.20 $\pm$ 0.91	69
CBIA-3 low								
$\gamma$ H2AX	5.56 $\pm$ 0.22	464	22.98 $\pm$ 0.38	523	21.87 $\pm$ 0.34	612	28.71 $\pm$ 0.34	554
53BP1	2.13 $\pm$ 0.12	445	8.76 $\pm$ 0.35	407	19.01 $\pm$ 0.31	552	23.1 $\pm$ 0.42	496
CBIA-3 high								
$\gamma$ H2AX	4.42 $\pm$ 0.20	483	17.91 $\pm$ 0.41	337	8.01 $\pm$ 0.27	594	7.97 $\pm$ 0.35	480
53BP1	1.46 $\pm$ 0.07	625	4.73 $\pm$ 0.18	510	14.45 $\pm$ 0.29	551	13.66 $\pm$ 0.31	447
CBIA-5 low								
$\gamma$ H2AX	5.69 $\pm$ 0.23	542	25.1 $\pm$ 0.47	415	28.6 $\pm$ 0.52	437	41.00 $\pm$ 0.55	421
53BP1	4.03 $\pm$ 0.18	445	15.3 $\pm$ 0.49	425	17.84 $\pm$ 0.26	613	23.32 $\pm$ 0.30	642
CBIA-5 high								
$\gamma$ H2AX	2.98 $\pm$ 0.13	520	10.98 $\pm$ 0.26	508	11.57 $\pm$ 0.27	445	24.45 $\pm$ 0.39	480
53BP1	1.56 $\pm$ 0.07	608	4.71 $\pm$ 0.21	461	8.04 $\pm$ 0.17	490	10.84 $\pm$ 0.20	514
CBIA-7 low								
$\gamma$ H2AX	5.89 $\pm$ 0.25	382	23.77 $\pm$ 0.45	414	26.48 $\pm$ 0.44	511	36.71 $\pm$ 0.52	444
53BP1	2.73 $\pm$ 0.13	487	10.42 $\pm$ 0.31	421	20.05 $\pm$ 0.35	591	21.94 $\pm$ 0.38	560
CBIA-7 high								
$\gamma$ H2AX	2.56 $\pm$ 0.13	547	11.78 $\pm$ 0.25	534	12.41 $\pm$ 0.26	580	12.73 $\pm$ 0.30	452
53BP1	1.51 $\pm$ 0.07	586	6.5 $\pm$ 0.27	415	16.9 $\pm$ 0.32	556	17.62 $\pm$ 0.34	415
CCTL-14 low								
$\gamma$ H2AX	4.45 $\pm$ 0.20	554	12.83 $\pm$ 0.31	544	20.99 $\pm$ 0.34	634	30.37 $\pm$ 0.57	378
53BP1	2.73 $\pm$ 0.14	629	10.28 $\pm$ 0.36	508	16.77 $\pm$ 0.27	681	19.13 $\pm$ 0.39	452
CCTL-14 high								
$\gamma$ H2AX	6.66 $\pm$ 0.29	510	19.30 $\pm$ 0.49	427	16.26 $\pm$ 0.28	642	19.38 $\pm$ 0.34	423
53BP1	4.75 $\pm$ 0.21	576	14.34 $\pm$ 0.52	402	21.49 $\pm$ 0.30	653	24.20 $\pm$ 0.42	425

The number of foci per cell and the number of analysed cells are shown for non-irradiated control cells and cells 0.5 h after irradiation with 1 Gy. Five samples were analysed: a fibroblast line (hDF), three hiPSC lines (CBIA-3, CBIA-5, and CBIA-7) and one hESC line (CCTL-14) at high or low passage number. The values are shown for the separated cell cycle phases G1 (EdU-negative) or S/G2 (EdU-positive)  
*EdU* 5-ethynyl-2'-deoxyuridine, *hDF* human dermal fibroblast

high-passage CBIA-5 cells. The percent increase of foci (both  $\gamma$ H2AX and 53BP1) after treatment with 1 Gy was higher in the cells in G1 phase than in those in S/G2 phase (Fig. 4b). Taken together, this set of data reveals that a high level of spontaneous DNA damage (replicative stress occurring in S/G2 phase) dramatically distorts the outcome of  $\gamma$ -irradiation as measured by the numbers of  $\gamma$ H2AX and 53BP1 foci.

As detailed above, we have found that irradiated high-passage hiPSCs load their DNA with much lower amounts of  $\gamma$ H2AX and 53BP1 than irradiated hDFs and low-passage hiPSCs, suggesting that high-passage hiPSCs are somewhat less proficient at initiating DNA repair. To

further examine this issue, we also determined the numbers of  $\gamma$ H2AX and 53BP1 foci at 2 and 6 h after  $\gamma$ -irradiation and then analysed the shapes of the resulting time-course curves. The steepness of the resulting curves, which are shown in Fig. 5a and b, collectively confirm our initial notion. The curves representing hDFs and low-passage hiPSCs decline more steeply, indicating a faster decrease in DSBs, while the curves representing high-passage hiPSCs decline more gradually, indicating slower recovery from DSBs.

We also analysed hESCs in parallel to hiPSCs to determine whether the studied phenomena are associated with de-differentiation to pluripotency or with the pluripotency

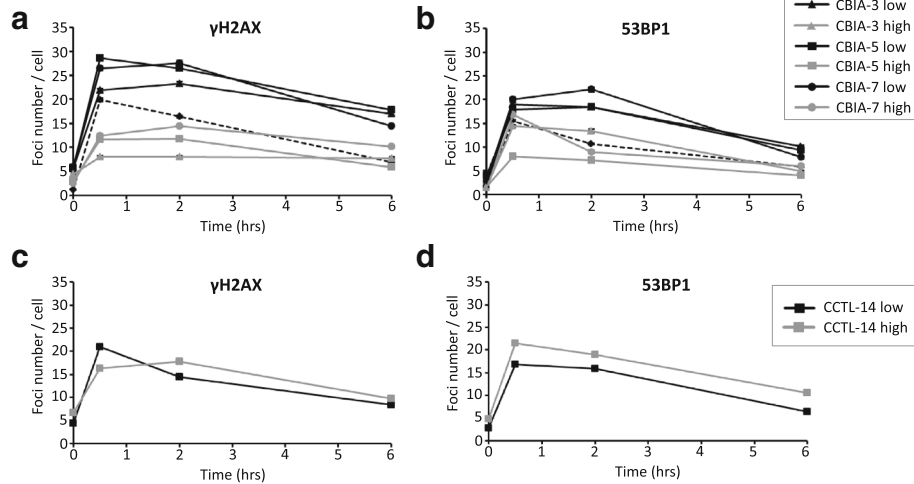


**Fig. 5** The time-course showing the recovery of human dermal fibroblasts (*hDFs*) and hiPSCs (**a,b**) or hESCs (**c,d**) after 1 Gy of  $\gamma$ -irradiation. **a,c** Number of DSBs recognized by  $\gamma$ H2AX and **b,d** by p53-binding protein 1 (*53BP1*) in the untreated control (0 h) and at 0.5 h, 2 h, and 6 h after irradiation with 1 Gy. The results are shown in the EdU-negative population. The mean value of the DSBs was calculated for each of the three regions on the slide. The error bar indicates the SEM

per se. Overall, the differences between irradiated low- and high-passage hESCs were much less pronounced than those in hiPSCs. This conclusion is substantiated by the numbers of: 1)  $\gamma$ H2AX foci in low- and high-passage EdU-negative hESCs (21.0 versus 16.3); 2) 53BP1 foci in low- and high-passage EdU-negative hESCs (16.8 versus 21.5) (Fig. 3c and d); 3)  $\gamma$ H2AX foci in low- and high-passage EdU-positive hESCs (30.4 versus 19.4); and 4) 53BP1 foci in low- and high-passage EdU-positive hESCs (19.1 versus 24.2) (Fig. 4a). It is of note that in high-passage hESCs (both EdU-negative and EdU-positive) the numbers of 53BP1 foci (but not of  $\gamma$ H2AX foci) even increased compared to those typical for low-passage hESCs. Finally, the steepness of the time-course curves indicated that the decrease was more similar to hDFs than to hiPSCs (Fig. 5c and d).

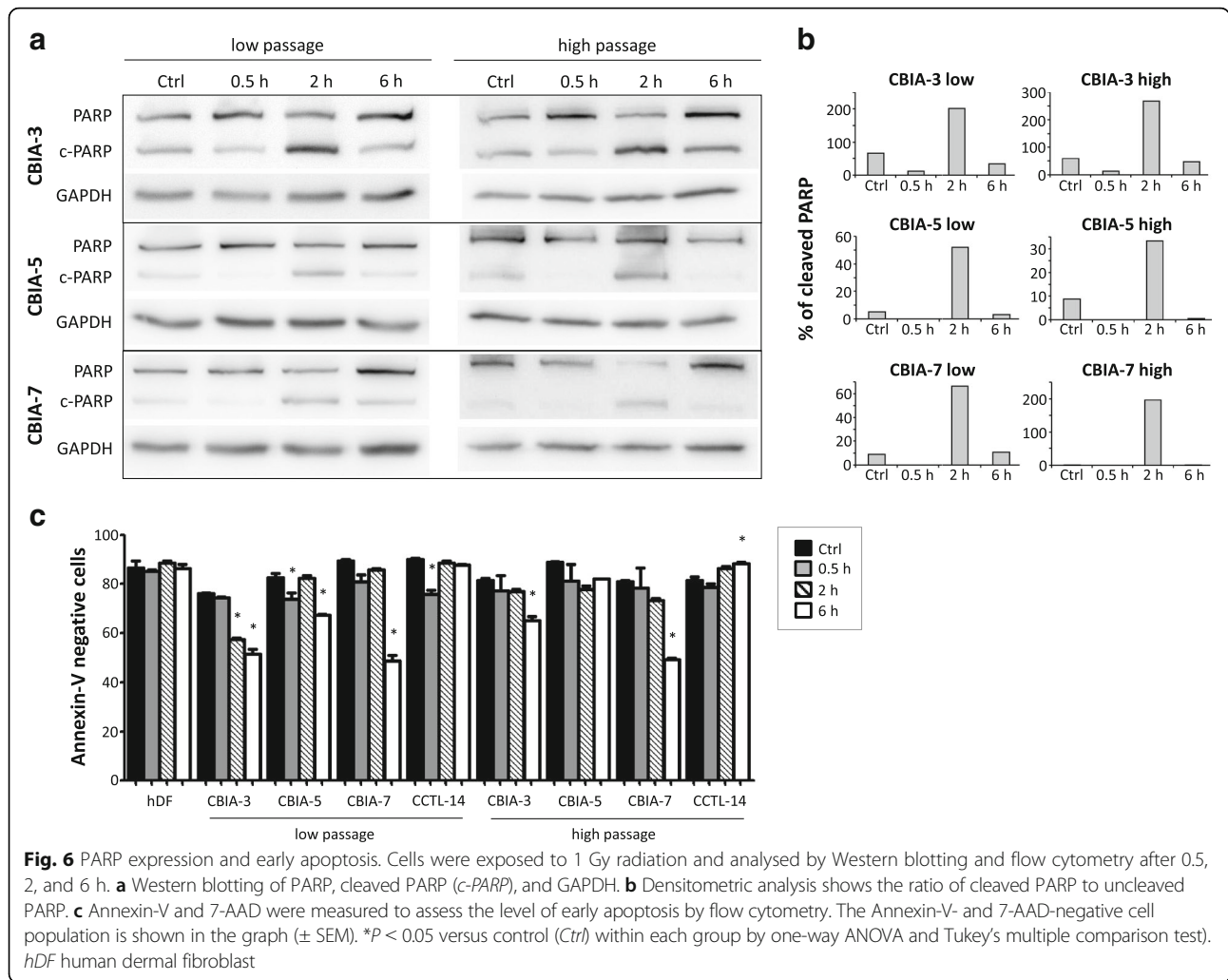
To test possible differences in the sensitivity of particular cell types to apoptotic signals, we investigated the cleavage of PARP, an indirect marker of DNA damage, and early apoptosis using Annexin-V/7-AAD assay. A Western blotting analysis of PARP in hiPSC lines demonstrated that the highest cleavage occurred at 2 h after  $\gamma$ -irradiation (Fig. 6a and b). No difference was observed between low and high passages. The PARP cleavage was later accompanied by a decrease in cell viability at the 6-h time-point in all hiPSC lines with the exception of high-passage CBIA-5 cells. Interestingly, hDFs and hESCs did not display as much sensitivity to 1 Gy  $\gamma$ -irradiation as hiPSCs (Fig. 6c).

### Discussion

A DNA molecule is unstable and subject to internal and external harmful factors. Correct functioning of the DNA repair mechanisms is, therefore, essential for the maintenance of genomic integrity. In the field of hiPSC research, only cells with an intact genome can be used for clinical application. Unfortunately, the generation and expansion of hiPSCs in vitro causes genomic instability. In our research, we monitored the amount of DSBs, either spontaneous or irradiation-induced, in three lines of hiPSCs (CBIA-3, CBIA-5, and CBIA-7) at low or high passage numbers, as well as in original source cell fibroblasts (hDFs). One hESC line (CCTL-14) was also examined. Our goal was to shed light on the reaction of the cells to reprogramming and on the prolonged in vitro culturing of pluripotent cells. Here, we focused specifically on the kinetics of DSB generation and repair, cell cycle speed changes, triggering of apoptosis, and cell viability. Special attention was paid to the cell cycle phase of individual cells.

We selected two markers of DSBs—the phosphorylated histone variant  $\gamma$ H2AX and its binding partner, the DNA repair mediator 53BP1. Fluorescence microscopy was chosen to detect these proteins because it offers two main advantages over other methods such as Western blotting. First, the expression of 53BP1 does not change; only its localization at DNA damage sites is affected. Second, analysis at the single-cell level assures a higher sensitivity and allows for the discrimination between cells at various cell cycle phases. We employed EdU staining, which discriminates between the G1 and S/G2





phases of the cell cycle. By incorporating a nucleoside analogue of thymidine (EdU) into the DNA during replication, only cells in the S or G2 stage are labelled positive [35]. The images were analysed using Acquarium software. This software allows us to reliably determine the foci number together with the intensity of the EdU signal for each individual cell and to analyse the data from hundreds of cells per sample on a large scale. Our method for separating EdU-negative (G1 phase) cells from EdU-positive (S/G2 phase) cells is based on plotting the EdU intensity levels in histograms and using the Otsu method to find the threshold. Using this method, we revealed a longer cell cycle in somatic cells compared to pluripotent cells, which is in accordance with previously published data [36–39] and justifies the use of this method for cell cycle discrimination on the single-cell level. This approach also assures consistency among samples.

While counting the numbers of  $\gamma$ H2AX and 53BP1 foci, it is of utmost importance to know exactly which phase of the cell cycle each individual cell is in at the

moment. Our data show that cells in S/G2 phase contain more  $\gamma$ H2AX and 53BP1 foci than cells in G1 phase and that this difference is more pronounced in non-irradiated controls. These foci emerge due to replication stress during S phase [12, 22, 23, 40]. The replication-related foci play a critical role in the comparison of DSB numbers, especially between different cell types. As long as the cells have a similar cell-cycle length (e.g. pluripotent cells at a similar passage number), the number of DSBs could be compared relatively well without using cell cycle discrimination. However, the following factors influence the cell cycle speed and should be considered: 1) pluripotent cells have been reported to have a shorter cell cycle than differentiated somatic cells [36–39]; 2) pluripotent cells at high passages may have an increased rate of proliferation [39, 41, 42]; and 3) irradiation induces cell cycle arrest through checkpoints [43–45]. We analysed the foci number separately for the EdU-negative and EdU-positive groups to eliminate the replication stress bias. Our data indicate a higher percent increase of foci upon

$\gamma$ -irradiation of cells in G1 phase, which are not burdened by replication-related foci. The cell-cycle dependency was confirmed for both  $\gamma$ H2AX and 53BP1 markers. In general, fewer foci were detected for 53BP1 than for  $\gamma$ H2AX, suggesting that 53BP1 is a less sensitive DSB marker with a lower capacity to recognize DSBs than  $\gamma$ H2AX. It is known that the HR pathway plays a pivotal role during hiPSC generation [46], and 53BP1 promotes the NHEJ repair pathway while inhibiting the HR pathway [19–21]. In contrast,  $\gamma$ H2AX influences both the NHEJ and HR pathways, and 53BP1 does not bind to all of the  $\gamma$ H2AX foci [10, 11, 18].

Similar research was performed by Suchánková et al. [25], who measured the formation of  $\gamma$ H2AX- and 53BP1-positive nuclear bodies in relation to cell cycle stages. They used genetically modified HeLa-Fucci cells, which are able to express RFP-Cdt1 in the G1 phase and GFP-geminin in the S/G2/M phases to discriminate among the cell cycle phases. They observed a higher number of  $\gamma$ H2AX-positive repair foci in the G2 phase than in the G1 phase for both non-irradiated and  $\gamma$ -irradiated (5 Gy) HeLa cells. In contrast to our work, they did not observe such a difference for 53BP1. It is of note that different cell types as well as a different radiation dose (1 Gy) were used in our study compared to Suchankova et al., and it has been previously published that foci formation upon ionizing radiation may vary between cell types and is radiation-dose dependent [32, 34, 47, 48].

In our study, we worked with three unique hiPSC lines that were derived from two independent cell types (dermal fibroblasts and blood cells) and reprogrammed either by the Sendai virus or episomal vectors. This selection of samples enables us to generalize our conclusions for hiPSCs to a certain extent. To avoid bias caused by replication-related foci, we further analysed  $\gamma$ H2AX and 53BP1 foci numbers only in the G1 (EdU-negative) subgroup. Our results indicate that spontaneously occurring DSBs are best recognized by both markers in hiPSCs at low passage, while fewer foci were observed in hiPSCs at high passage and in source fibroblasts. A low foci number in fibroblasts, therefore, is increased significantly after reprogramming into hiPSCs (either by Sendai virus or episomal vectors) and then decreases again after long-term in vitro passaging. Our results are consistent with recently reported data showing that H2AX plays a critical role in iPSC generation. González et al. reported an increase in  $\gamma$ H2AX during the cellular reprogramming of mouse embryonic fibroblasts independent of viral integration [46]. The HR pathway was confirmed to be essential for the error-free repair of DSBs in both genome-integrating and non-integrating reprogramming. The importance of H2AX at the early stage of reprogramming was also suggested by Wu et al. [49]. Our observations markedly

resemble the results of copy number variation (CNV) measurements by Hussein et al. [50]. They concluded that most de novo-formed CNVs are present in early-passage hiPSCs, while fewer CNVs are found in late-passage hiPSCs and fibroblasts. There is a strong connection between CNVs and DSBs because deletions in subtelomeric regions have been shown to be highly sensitive to DSBs and are the major cause of chromosomal instability [51, 52]. Similar results were published by Laurent et al. [7] who reported a higher frequency of CNVs in pluripotent samples than in non-pluripotent samples and noticed that some of the deletions receded from the population over long-term passaging. Taken together, their data suggest that genomic instability is highest in low-passage hiPSCs, and CNVs vanish during multiple clonal-based passages because most of the mutations do not provide any advantage. However, certain growth-advantageous mutations—for example, defects in genes controlling the cell cycle—may be fixed in the population [5].

The abovementioned findings imply that more DSBs at low passages are detected as a consequence of reprogramming stress and disappear as the hiPSCs are adapted to in vitro conditions and clonally selected. However, the irradiation experiments revealed that the high-passage hiPSCs cannot recognize DSBs as effectively as hDF source cells, particularly by  $\gamma$ H2AX. The lack of ability to recognize the irradiation-induced DSBs was also obvious in all three high-passage hiPSCs lines in the time-course study. These data suggest that hiPSCs lose their repair capacity over multiple passages in vitro. Similar results were published by Zhang et al. on one mouse iPSC line [29]. They confirmed the compromised DNA damage repair capacity of iPSCs compared with the respective source cells after  $\gamma$ -irradiation treatment but did not focus on the length of the in vitro culturing of iPSCs. For potential clinical applications, the length of in vitro culturing time should be reduced to as short as possible. However, a certain amount of time in vitro is unavoidable because of the reprogramming process itself, cell expansion, and clearance of the remaining reprogramming factors (viral particles or vectors).

Of note, low- and high-passage hiPSCs displayed similar apoptotic responses upon  $\gamma$ -irradiation. PARP cleavage peaked 2 h after irradiation, which led to an increase in early apoptosis after an additional 4 h in most of the hiPSC lines. These data suggest that, despite differences in DSB recognition, both low- and high-passage hiPSCs exert DNA protection mechanisms that trigger apoptosis in reaction to  $\gamma$ -irradiation. Increased apoptosis was not observed in somatic hDFs or in the hESC line CCTL-14, suggesting their lower sensitivity to DNA damage.

## Conclusions

This study addresses the question of hiPSC capability to repair their DNA using three independent lines of hiPSCs. It shows for the first time that: 1) reprogramming to pluripotency increases the number of DNA double-strand breaks (DSBs) as recognized by the  $\gamma$ H2AX and 53BP1 proteins; 2) these DSBs are not due to replicative stress to DNA; and 3) their numbers become reduced during prolonged propagation after reprogramming. It also shows that prolonged passaging of hiPSCs is associated with a decrease in their DNA repair capacity and that this is not the case for the hESC line CCTL-14. From a technical point of view, this study documents that solid accuracy in analysing numbers of DSBs requires discrimination between the cells in G1 and S/G2 phases of their cell cycle. Collectively, hiPSCs at low passage contain more DSBs than hiPSCs at high passage, but they can repair them more efficiently.

## Additional files

**Additional file 1: Figure S1.** Immunocytochemistry of pluripotency markers. The pluripotency markers Oct-3/4, Sox2, Nanog, and SSEA4 are highly expressed in all three hiPSC lines used in this study (CBIA-3, CBIA-5, and CBIA-7). An anti-mouse secondary antibody conjugated with Alexa Fluor® 488 was used to detect Oct-3/4, Sox2, and SSEA4. An anti-rabbit secondary antibody conjugated with Alexa Fluor® 488 was used to detect Nanog. Scale bar = 100  $\mu$ m. (PPTX 384 kb)

**Additional file 2: Figure S2.** Histological staining of a teratoma. Cell types representative of the three germ layers were detected by histological analysis in the CBIA-7 hiPSC cell line at passage number 26. (A) Glandular structures with secretory cells (endoderm); (B) mesenchymal cells (mesoderm); (C) cells with melanin (ectoderm); (D) glomerulus-like cells (mesoderm). (PPTX 32103 kb)

**Additional file 3: Figure S3.** Histograms of EdU signal intensity. The distribution of the EdU-negative and EdU-positive populations in hDF source cells, hiPSCs (CBIA-3, CBIA-5, and CBIA-7) and hESCs (CCTL-14) at low or high passage is shown. The samples were fixed 0.5 h, 2 h, and 6 h after 1 Gy of  $\gamma$ -irradiation. The thresholds for the EdU-negative population were calculated as described in the Methods section and are marked with a dotted line. (PPTX 251 kb)

## Abbreviations

53BP1: p53-Binding protein 1; 7-AAD: 7-Amino-actinomycin D; ANOVA: One-way analysis of variance; CNV: Copy number variation; DSB: Double-strand break; EdU: 5-Ethynyl-2'-deoxyuridine; FITC: Fluorescein isothiocyanate; hDF: Human dermal fibroblast; hESC: Human embryonic stem cell; hiPSC: Human induced pluripotent stem cell; HR: Homologous recombination; IR: Ionizing radiation; MEF: Mouse embryonic fibroblast; NHEJ: Non-homologous end-joining; p: Passage; PSC: Pluripotent stem cell

## Acknowledgements

The authors are very grateful to colleagues from the Department of Histology and Embryology, Faculty of Medicine, Masaryk University, Brno, Czech Republic, for assistance during the teratoma assay. We thank our colleagues from the National Tissue Centre, Brno, for the generous gift of fibroblast cells. We are grateful to Z. Racil from the Department of Internal Medicine, Haematology and Oncology, Masaryk University and University Hospital, Brno, for providing blood samples. We thank American Journal Experts for their editorial services.

## Funding

This study was generously supported by the Grant Agency of the Czech Republic (302/12/G157) and by the Czech Health Research Council (16-31501A).

## Availability of data and materials

All datasets supporting this article have been uploaded as part of the Additional files.

## Authors' contributions

PS was responsible for conception and design, collection and assembly of data, data analysis and interpretation, and manuscript writing. LT was responsible for conception and design, data analysis and interpretation, and manuscript writing. DR was responsible for collection and assembly of data, and data analysis and interpretation. PM was responsible for collection and assembly of data, data analysis and interpretation, and manuscript writing. SS was responsible for collection and assembly of data, data analysis and interpretation, and manuscript writing. AH was responsible for conception and design, data analysis and interpretation, and manuscript writing. IK was responsible for conception and design, data analysis and interpretation, and manuscript writing. All authors read and approved the final manuscript.

## Competing interests

The authors declare that they have no competing interests.

## Consent for publication

Not applicable.

## Ethics approval and consent to participate

Human tissue samples were collected under approved guidelines set by the Faculty of Medicine, Masaryk University, Brno, and by the National Tissue Centre, Brno. All patients signed an informed consent form.

## Author details

<sup>1</sup>Centre for Biomedical Image Analysis, Faculty of Informatics, Masaryk University, Kamenice 5, 625 00 Brno, Czech Republic. <sup>2</sup>Department of Histology and Embryology, Faculty of Medicine, Masaryk University, Kamenice 3, 625 00 Brno, Czech Republic.

Received: 21 September 2016 Revised: 9 February 2017

Accepted: 24 February 2017 Published online: 21 March 2017

## References

- Takahashi K, Yamanaka S. Induction of pluripotent stem cells from mouse embryonic and adult fibroblast cultures by defined factors. *Cell*. 2006;126:663–76.
- Takahashi K, Tanabe K, Ohnuki M, Narita M, Ichisaka T, Tomoda K, Yamanaka S. Induction of pluripotent stem cells from adult human fibroblasts by defined factors. *Cell*. 2007;131:861–72.
- Yu J, Vodyanik MA, Smuga-Otto K, Antosiewicz-Bourget J, Frane JL, Tian S, Nie J, Jonsdottir GA, Ruotti V, Stewart R, et al. Induced pluripotent stem cell lines derived from human somatic cells. *Science*. 2007;318:1917–20.
- Simara P, Motl JA, Kaufman DS. Pluripotent stem cells and gene therapy. *Transl Res*. 2013;161:284–92.
- Weissbein U, Benvenisty N, Ben-David U. Quality control: genome maintenance in pluripotent stem cells. *J Cell Biol*. 2014;204:153–63.
- Gore A, Li Z, Fung HL, Young JE, Agarwal S, Antosiewicz-Bourget J, Canto I, Giorgetti A, Israel MA, Kiskinis E, et al. Somatic coding mutations in human induced pluripotent stem cells. *Nature*. 2011;471:63–7.
- Laurent LC, Ulitsky I, Slavin I, Tran H, Schork A, Morey R, Lynch C, Harness JV, Lee S, Barrero MJ, et al. Dynamic changes in the copy number of pluripotency and cell proliferation genes in human ESCs and iPSCs during reprogramming and time in culture. *Cell Stem Cell*. 2011;8:106–18.
- Cheng L, Hansen NF, Zhao L, Du Y, Zou C, Donovan FX, Chou BK, Zhou G, Li S, Dowey SN, et al. Low incidence of DNA sequence variation in human induced pluripotent stem cells generated by nonintegrating plasmid expression. *Cell Stem Cell*. 2012;10:337–44.
- Taapken SM, Nisler BS, Newton MA, Sampsell-Barron TL, Leonhard KA, McIntire EM, Montgomery KD. Karyotypic abnormalities in human induced pluripotent stem cells and embryonic stem cells. *Nat Biotechnol*. 2011;29:313–4.
- Shrivastav M, De Haro LP, Nickoloff JA. Regulation of DNA double-strand break repair pathway choice. *Cell Res*. 2008;18:134–47.

11. Rothkamm K, Krüger I, Thompson LH, Löbrich M. Pathways of DNA double-strand break repair during the mammalian cell cycle. *Mol Cell Biol.* 2003;23:5706–15.
12. Adams BR, Golding SE, Rao RR, Valerie K. Dynamic dependence on ATR and ATM for double-strand break repair in human embryonic stem cells and neural descendants. *PLoS One.* 2010;5:e10001.
13. Tichy ED, Pillai R, Deng L, Liang L, Tischfield J, Schwemberger SJ, Babcock GF, Stambrook PJ. Mouse embryonic stem cells, but not somatic cells, predominantly use homologous recombination to repair double-strand DNA breaks. *Stem Cells Dev.* 2010;19:1699–711.
14. Maynard S, Swistowska AM, Lee JW, Liu Y, Liu ST, Da Cruz AB, Rao M, de Souza-Pinto NC, Zeng X, Bohr VA. Human embryonic stem cells have enhanced repair of multiple forms of DNA damage. *Stem Cells.* 2008;26:2266–74.
15. Rothkamm K, Barnard S, Moquet J, Ellender M, Rana Z, Burdak-Rothkamm S. DNA damage foci: meaning and significance. *Environ Mol Mutagen.* 2015;56:491–504.
16. Panier S, Boulton SJ. Double-strand break repair: 53BP1 comes into focus. *Nat Rev Mol Cell Biol.* 2014;15:7–18.
17. Rogakou EP, Pilch DR, Orr AH, Ivanova VS, Bonner WM. DNA double-stranded breaks induce histone H2AX phosphorylation on serine 139. *J Biol Chem.* 1998;273:5858–68.
18. Kleiner RE, Verma P, Molloy KR, Chait BT, Kapoor TM. Chemical proteomics reveals a  $\gamma$ H2AX-53BP1 interaction in the DNA damage response. *Nat Chem Biol.* 2015;11:807–14.
19. Bunting SF, Callén E, Wong N, Chen HT, Polato F, Gunn A, Bothmer A, Feldhahn N, Fernandez-Capetillo O, Cao L, et al. 53BP1 inhibits homologous recombination in Brca1-deficient cells by blocking resection of DNA breaks. *Cell.* 2010;141:243–54.
20. Dimitrova N, Chen YC, Spector DL, de Lange T. 53BP1 promotes non-homologous end joining of telomeres by increasing chromatin mobility. *Nature.* 2008;456:524–8.
21. Zimmermann M, Lotterberger F, Buonomo SB, Sfeir A, de Lange T. 53BP1 regulates DSB repair using Rif1 to control 5' end resection. *Science.* 2013;339:700–4.
22. Huang X, Tanaka T, Kurose A, Traganos F, Darzynkiewicz Z. Constitutive histone H2AX phosphorylation on Ser-139 in cells untreated by genotoxic agents is cell-cycle phase specific and attenuated by scavenging reactive oxygen species. *Int J Oncol.* 2006;29:495–501.
23. MacPhail SH, Banáth JP, Yu Y, Chu E, Olive PL. Cell cycle-dependent expression of phosphorylated histone H2AX: reduced expression in unirradiated but not X-irradiated G1-phase cells. *Radiat Res.* 2003;159:759–67.
24. Dale Rein I, Stokke C, Jalal M, Myklebust JH, Patzke S, Stokke T. New distinct compartments in the G2 phase of the cell cycle defined by the levels of  $\gamma$ H2AX. *Cell Cycle.* 2015;14:3261–9.
25. Suchánková J, Kozubek S, Legartová S, Sehnalová P, Kuntziger T, Bártoš E. Distinct kinetics of DNA repair protein accumulation at DNA lesions and cell cycle-dependent formation of  $\gamma$ H2AX- and NBS1-positive repair foci. *Biol Cell.* 2015;107:440–54.
26. Šimara P, Tesařová L, Padourová S, Koutná I. Generation of human induced pluripotent stem cells using genome integrating or non-integrating methods. *Folia Biol.* 2014;60:85–9.
27. Tesařová L, Šimara P, Stejskal S, Koutná I. Haematopoietic developmental potential of human pluripotent stem cell lines. *Folia Biol.* 2014;60:90–4.
28. Adewumi O, Aflatoonian B, Ahrlund-Richter L, Amit M, Andrews PW, Beighton G, Bello PA, Benvenisty N, Berry LS, Bevan S, et al. Characterization of human embryonic stem cell lines by the International Stem Cell Initiative. *Nat Biotechnol.* 2007;25:803–16.
29. Zhang M, Yang C, Liu H, Sun Y. Induced pluripotent stem cells are sensitive to DNA damage. *Genomics Proteomics Bioinformatics.* 2013;11:320–6.
30. Matula P, Maška M, Daněk O, Matula P, Kozubek M. Acquarium: free software for acquisition and analysis of 3D images of cells in fluorescence microscopy. In: 6th IEEE International Symposium on Biomedical Imaging. Boston. 2009.
31. Štěpka K, Matula P, Wörz S, Rohr K, Kozubek M. Performance and sensitivity evaluation of 3D spot detection methods in confocal microscopy. *Cytometry A.* 2015;87:759–72.
32. Schultz LB, Chehab NH, Malikzay A, Halazonetis TD. p53 binding protein 1 (53BP1) is an early participant in the cellular response to DNA double-strand breaks. *J Cell Biol.* 2000;151:1381–90.
33. Rogakou EP, Boon C, Redon C, Bonner WM. Megabase chromatin domains involved in DNA double-strand breaks in vivo. *J Cell Biol.* 1999;146:905–16.
34. Redon CE, Dickey JS, Bonner WM, Sedelnikova OA.  $\gamma$ -H2AX as a biomarker of DNA damage induced by ionizing radiation in human peripheral blood lymphocytes and artificial skin. *Adv Space Res.* 2009;43:1171–8.
35. Salic A, Mitchison TJ. A chemical method for fast and sensitive detection of DNA synthesis in vivo. *Proc Natl Acad Sci U S A.* 2008;105:2415–20.
36. Stead E, White J, Faast R, Conn S, Goldstone S, Rathjen J, Dhingra U, Rathjen P, Walker D, Dalton S. Pluripotent cell division cycles are driven by ectopic Cdk2, cyclin A/E and E2F activities. *Oncogene.* 2002;21:8320–33.
37. Becker KA, Ghule PN, Therrien JA, Lian JB, Stein JL, van Wijnen AJ, Stein GS. Self-renewal of human embryonic stem cells is supported by a shortened G1 cell cycle phase. *J Cell Physiol.* 2006;209:883–93.
38. Calder A, Roth-Albin I, Bhatia S, Pilquil C, Lee JH, Bhatia M, Levadoux-Martin M, McNicol J, Russell J, Collins T, et al. Lengthened G1 phase indicates differentiation status in human embryonic stem cells. *Stem Cells Dev.* 2013;22:279–95.
39. Barta T, Dolezalova D, Holubcova Z, Hampl A. Cell cycle regulation in human embryonic stem cells: links to adaptation to cell culture. *Exp Biol Med.* 2013;238:271–5.
40. Suzuki K, Okada H, Yamauchi M, Okayama Y, Kodama S, Watanabe M. Qualitative and quantitative analysis of phosphorylated ATM foci induced by low-dose ionizing radiation. *Radiat Res.* 2006;165:499–504.
41. Werbowetski-Ogilvie TE, Bossé M, Stewart M, Schnerch A, Ramos-Mejia V, Rouleau A, Wynder T, Smith MJ, Dingwall S, Carter T, et al. Characterization of human embryonic stem cells with features of neoplastic progression. *Nat Biotechnol.* 2009;27:91–7.
42. Yang S, Lin G, Tan YQ, Zhou D, Deng LY, Cheng DH, Luo SW, Liu TC, Zhou XY, Sun Z, et al. Tumor progression of culture-adapted human embryonic stem cells during long-term culture. *Genes Chromosomes Cancer.* 2008;47:665–79.
43. Hartwell LH, Weinert TA. Checkpoints: controls that ensure the order of cell cycle events. *Science.* 1989;246:629–34.
44. Kastan MB, Onyekwere O, Sidransky D, Vogelstein B, Craig RW. Participation of p53 protein in the cellular response to DNA damage. *Cancer Res.* 1991;51:6304–11.
45. Kuerbitz SJ, Plunkett BS, Walsh WW, Kastan MB. Wild-type p53 is a cell cycle checkpoint determinant following irradiation. *Proc Natl Acad Sci U S A.* 1992;89:7491–5.
46. González F, Georgieva D, Vanoli F, Shi ZD, Stadtfeld M, Ludwig T, Jasin M, Huangfu D. Homologous recombination DNA repair genes play a critical role in reprogramming to a pluripotent state. *Cell Rep.* 2013;3:651–60.
47. Raschke S, Spickermann S, Toncian T, Swantusch M, Boeker J, Giesen U, Iliakis G, Willi O, Boege F. Ultra-short laser-accelerated proton pulses have similar DNA-damaging effectiveness but produce less immediate nitrooxidative stress than conventional proton beams. *Sci Rep.* 2016;6:32441.
48. Woodward WA, Chen MS, Behbod F, Alfaro MP, Buchholz TA, Rosen JM. WNT/beta-catenin mediates radiation resistance of mouse mammary progenitor cells. *Proc Natl Acad Sci U S A.* 2007;104:618–23.
49. Wu T, Liu Y, Wen D, Tseng Z, Tahmasian M, Zhong M, Rafii S, Stadtfeld M, Hochdinger K, Xiao A. Histone variant H2AX deposition pattern serves as a functional epigenetic mark for distinguishing the developmental potentials of iPSCs. *Cell Stem Cell.* 2014;15:281–94.
50. Hussein SM, Batada NN, Vuoristo S, Ching RW, Autio R, Närvä E, Ng S, Sourour M, Hämäläinen R, Olsson C, et al. Copy number variation and selection during reprogramming to pluripotency. *Nature.* 2011;471:58–62.
51. Kulkarni A, Zschenker O, Reynolds G, Miller D, Murnane JP. Effect of telomere proximity on telomere position effect, chromosome healing, and sensitivity to DNA double-strand breaks in a human tumor cell line. *Mol Cell Biol.* 2010;30:578–89.
52. Zschenker O, Kulkarni A, Miller D, Reynolds GE, Granger-Locatelli M, Pottier G, Sabatier L, Murnane JP. Increased sensitivity of subtelomeric regions to DNA double-strand breaks in a human cancer cell line. *DNA Repair.* 2009;8:886–900.

# Reprogramming of Adult Peripheral Blood Cells into Human Induced Pluripotent Stem Cells as a Safe and Accessible Source of Endothelial Cells

Pavel Simara,<sup>1</sup> Lenka Tesarova,<sup>1,2</sup> Daniela Rehakova,<sup>1</sup> Simon Farkas,<sup>1</sup> Barbara Salingova,<sup>1</sup>  
Katerina Kutalkova,<sup>1</sup> Eva Vavreckova,<sup>1</sup> Pavel Matula,<sup>1</sup> Petr Matula,<sup>1</sup>  
Lenka Veverkova,<sup>3</sup> and Irena Koutna<sup>1,2</sup>

New approaches in regenerative medicine and vasculogenesis have generated a demand for sufficient numbers of human endothelial cells (ECs). ECs and their progenitors reside on the interior surface of blood and lymphatic vessels or circulate in peripheral blood; however, their numbers are limited, and they are difficult to expand after isolation. Recent advances in human induced pluripotent stem cell (hiPSC) research have opened possible avenues to generate unlimited numbers of ECs from easily accessible cell sources, such as the peripheral blood. In this study, we reprogrammed peripheral blood mononuclear cells, human umbilical vein endothelial cells (HUVECs), and human saphenous vein endothelial cells (HSVECs) into hiPSCs and differentiated them into ECs. The phenotype profiles, functionality, and genome stability of all hiPSC-derived ECs were assessed and compared with HUVECs and HSVECs. hiPSC-derived ECs resembled their natural EC counterparts, as shown by the expression of the endothelial surface markers CD31 and CD144 and the results of the functional analysis. Higher expression of endothelial progenitor markers CD34 and kinase insert domain receptor (KDR) was measured in hiPSC-derived ECs. An analysis of phosphorylated histone H2AX ( $\gamma$ H2AX) foci revealed that an increased number of DNA double-strand breaks upon reprogramming into pluripotent cells. However, differentiation into ECs restored a normal number of  $\gamma$ H2AX foci. Our hiPSCs retained a normal karyotype, with the exception of the HSVEC-derived hiPSC line, which displayed mosaicism due to a gain of chromosome 1. Peripheral blood from adult donors is a suitable source for the unlimited production of patient-specific ECs through the hiPSC interstage. hiPSC-derived ECs are fully functional and comparable to natural ECs. The protocol is eligible for clinical applications in regenerative medicine, if the genomic stability of the pluripotent cell stage is closely monitored.

**Keywords:** induced pluripotent stem cells, endothelial differentiation, peripheral blood mononuclear cells

## Introduction

ENDOTHELIAL CELLS (ECs) form a thin layer on the interior surface of blood and lymphatic vessels. They regulate various physiological processes, such as blood hemostasis, vascular tone, interaction of the vessel wall with blood elements, and the formation of new blood vessels [1]. On the contrary, ECs are involved in pathological states, such as cancer, atherosclerosis, and other diseases [2,3]. Therefore, ECs represent an important *in vitro* model for studies of vascular development and drug screens [4,5]. In regenerative medicine, ECs have been used to generate the cellular lining of vascular grafts [6,7]. Currently, several clinical trials are

being conducted on endothelial progenitor cells (EPCs), mainly as myocardial infarction and peripheral vascular disease treatments (reviewed in Chong et al. [8]).

The first human ECs were isolated from umbilical cord [human umbilical vein endothelial cells (HUVECs)] [9] and became a popular model for vascular research. Adult ECs are also commonly isolated from saphenous vein [human saphenous vein endothelial cells (HSVECs)] [10], usually from patients undergoing bypass or varicose vein surgery. ECs used for the treatment of ischemic conditions or other diseases are mainly populations of circulating EPCs that are usually positive for CD34 surface marker alone or in combination with kinase insert domain receptor (KDR; also

<sup>1</sup>Centre for Biomedical Image Analysis, Faculty of Informatics, Masaryk University, Brno, Czech Republic.

<sup>2</sup>International Clinical Research Center, St. Anne's University Hospital Brno, Brno, Czech Republic.

<sup>3</sup>I. Surgery Department, St. Anne's University Hospital Brno, Brno, Czech Republic.



known as vascular endothelial growth factor receptor 2; VEGFR-2) or CD133 [11–13]. However, ECs from blood vessels or peripheral blood can be obtained in limited numbers and are difficult to expand. To overcome these hurdles, pluripotent stem cells (PSCs) can be used. In vitro methods for EC production from PSCs have been recently introduced. This approach ensures a consistent and potentially unlimited source of ECs for in vitro studies and regenerative medicine.

The key question to be addressed is if PSC-derived ECs are comparable to ECs isolated from human tissues and safe for future clinical applications. Both human embryonic stem cells (hESCs) and human induced pluripotent stem cells (hiPSCs) have the capacity to differentiate into ECs [14–21]. In contrast to hESCs, hiPSCs are easier to obtain and do not generate ethical controversy. The first hiPSCs were created from skin fibroblasts [22,23], and this cell type is still among the most frequently used source of hiPSC. However, uncomfortable procedures for harvesting skin biopsies and the time requirements for establishing fibroblast cell lines limit the use of fibroblasts for reprogramming.

Peripheral blood overcomes these issues and the quality of hiPSC derived from mononuclear cells [peripheral blood mononuclear cells (PBMCs)] and those derived from fibroblasts is equivalent, indistinguishable from hESCs [24]. Several methods for PBMCs reprogramming have been published [24–30], varying mainly in the type of reprogramming vectors and media used for ex vivo PBMCs expansion. The composition of the expansion media containing the optimal cocktail of cytokines is the crucial factor for successful reprogramming. Preferential induction of the proliferation of hematopoietic progenitor cells, as described in Shah et al. [31], may be the key factor in highly efficient routine PBMCs reprogramming.

The potential of hiPSC-based therapies in regenerative medicine is hindered by genomic instability. The processes of cellular reprogramming and subsequent in vitro culture of hiPSCs have been reported to compromise genomic stability, particularly through introduction of DNA double-strand breaks (DSBs) [32–35]. The genome instability in PSCs may eventually result in karyotypic abnormalities, such as chromosomal and subchromosomal aberrations. Gains of chromosomes 1, 12, 17, 20, and X represent the most common events observed in hESCs and hiPSCs (summarized in Weissbein et al. [36]).

In our study, we reprogrammed PBMCs, HUVECs, and HSVECs with episomal vectors and subsequently created hiPSC-derived ECs. Our goal was to verify that hiPSC-derived ECs are phenotypically and functionally comparable to HUVECs and HSVECs. Genomic stability was a high priority during the reprogramming/differentiation process; therefore, the numbers of DSBs were measured by counting phosphorylated histone H2AX ( $\gamma$ H2AX) foci, together with a karyotype analysis. Experiments were conducted in a virus-free and DNA nonintegrating setting without feeder cells, which are the main criteria for future clinical applications.

## Materials and Methods

### *Ethics approval and consent to participate*

Studies were performed according to the amended Declaration of Helsinki. Institutional Review Board of the St. Anne's University Hospital Brno and the Faculty of Medicine, Masaryk University Brno approved the protocol used in our study,

including the use of human PSCs. All patients gave written informed consent. Protocols for teratoma studies in animals were reviewed and approved by the Institutional Review Board at the Faculty of Medicine, Masaryk University Brno and conformed to the national guidelines of the Czech Republic.

### *Cell isolation and culture*

Peripheral blood samples and pieces of saphenous vein were collected from patients undergoing varicose vein surgery. PBMCs were isolated from 6 mL of peripheral blood using Histopaque-1077 density gradient centrifugation (Sigma-Aldrich, St. Louis, MO). The total count of isolated PBMCs was  $7.4 \times 10^6$ . Before reprogramming, PBMCs were cultured on low-attachment culture dish in complete PBMC medium (cPBMC) consisting of StemPro<sup>®</sup>-34 serum-free medium, supplemented with 2 mM L-Glutamine (both from Thermo Fisher Scientific, Waltham, MA), ZellShield<sup>®</sup> (Minerva Biolabs, Berlin, Germany) and the growth factors stem cell factor (SCF), flt-3 Ligand (Flt-3L; both 100 ng/mL), interleukin (IL)-3 (20 ng/mL), and IL-6 (10 ng/mL; all from Peprotech, Rocky Hill, NJ) for 3 days. The initial seeding density was  $2 \times 10^5$  cells/cm<sup>2</sup>.

An ~10 cm-long piece of human saphenous vein was washed with phosphate-buffered saline (PBS) and cut into 1.5–2 cm-long pieces. Vein samples were incubated with 0.3% Collagenase II (Thermo Fisher Scientific) in Hank's medium (Sigma-Aldrich) for 50 min in a humidified 37°C incubator with an atmosphere of 5% (v/v) CO<sub>2</sub>. The cells from the digested tissue were washed with medium, centrifuged and seeded on T25 EasYFlasks<sup>™</sup> (Thermo Fisher Scientific) in Endothelial Growth Medium-2 (EGM-2; Lonza, Basel, Switzerland) supplemented with 10% fetal bovine serum (FBS; Sigma-Aldrich) and ZellShield (Minerva Biolabs) at a density of  $3.5 \times 10^4$  cells/cm<sup>2</sup>. After the first passage, the cells were cultured on tissue-culture plates coated with 0.1% gelatin. Passaging was performed using trypsin/EDTA (0.5 mg/mL trypsin with 0.2 mg/mL EDTA; Sigma-Aldrich) when cells reached ~90% confluence. HUVECs were purchased from Thermo Fisher Scientific and maintained under the same conditions as HSVECs.

### *Generation of hiPSCs*

hiPSCs were generated from PBMCs (hiPSC-PB; line ID CBIA-26), HUVECs (hiPSC-HU; line ID CBIA-19), and HSVECs (hiPSC-HS; line ID CBIA-25), using genome non-integrating episomal vectors (Epi5<sup>™</sup> Episomal hiPSC Reprogramming Kit; Thermo Fisher Scientific), according to the manufacturer's instructions. In brief, reprogramming factors (Oct3/4, Sox2, Klf4, Lin28, and c-Myc) were delivered in episomal vectors with an oriP/EBNA-1 (Epstein-Barr nuclear antigen-1) backbone [37]. Electroporation was performed at 1,600 V in three pulses for 10 ms for  $2 \times 10^5$  cells in the Neon electroporator (Thermo Fisher Scientific).

Reprogrammed cells were then seeded at a density of  $2 \times 10^4$  cells/cm<sup>2</sup> on plates that had been precoated with the Matrigel<sup>™</sup> matrix (Thermo Fisher Scientific) in cPBMC medium for PBMCs or in EGM-2 for HUVECs and HSVECs. At day 7 after reprogramming, the medium was changed to mTeSR<sup>™</sup> 1 (Stemcell Technologies, Vancouver, Canada). hiPSC colonies were mechanically picked from days 17 to 25 and transferred to separate wells of a 12-well plate.

Subsequent passaging was performed using 0.5 mM EDTA (Thermo Fisher Scientific). One hour before passaging, the cells were pretreated with 10  $\mu$ M Y-27632 (ROCK inhibitor; Selleckchem, Houston, TX). hiPSCs were maintained on tissue-culture plates that had been precoated with Matrigel in mTeSR1 medium supplemented with ZellShield. The medium was changed daily.

### *Immunocytochemistry*

Pluripotency markers were detected with primary antibodies against Oct3/4 (Santa Cruz Biotechnology, Dallas, TX), Sox2 (R&D Systems, Minneapolis, MN), and Nanog (Cell Signaling Technology, Danvers, MA) as previously described [38]. In brief, cells on plates were fixed with 4% paraformaldehyde and permeabilized with 0.2% Triton X-100 (both from Sigma-Aldrich). Cells were incubated with primary antibodies overnight at 4°C, followed by 2-h incubation with secondary antibody conjugated with Alexa 488 (Cell Signaling Technology). Nuclei were stained with Hoechst dye (bisbenzimidazole H33258; 1  $\mu$ g/mL; Sigma-Aldrich). Fluorescent signals were detected under an inverted Olympus IX71 microscope (Olympus, Hamburg, Germany).

### *Flow cytometry*

Flow cytometry was used to determine the expression of cell surface antigens. Specifically, antibodies against the pluripotency markers SSEA-4 (Phycoerythrin-conjugated antibody; PE; clone MC-813-70; R&D Systems) as well as Tra-1-60 and Tra-1-81 (both PE; REA157, resp. REA246; both from Miltenyi Biotec, Bergisch Gladbach, Germany) were used. The expression of CD31 (Allophycocyanin-conjugated antibody; APC; AC128; Miltenyi Biotec), CD34 (PE; AC136; Miltenyi Biotec), CD144 (PE; REA199; Miltenyi Biotec), and KDR (PE; ES8-20E6; Miltenyi Biotec) and the uptake of dil-labeled and acetylated low-density lipoprotein (Dil-Ac-LDL; Alpha Diagnostics, San Antonio, TX) were measured to characterize ECs. For isotype controls were used antibodies Mouse IgG3 (PE; 133316; R&D Systems), REA Control (PE; REA293; Miltenyi Biotec), and Mouse IgG1 (APC; IS5-21F5; Miltenyi Biotec).

Cells were harvested as a single-cell suspension using trypsin/EDTA and resuspended in PBS containing 0.5% bovine serum albumin and 2 mM EDTA. Cells were incubated with fluorochrome-conjugated antibodies for 30 min at 4°C, followed by washes with PBS. Cells were incubated with 10  $\mu$ g/mL Dil-Ac-LDL for 4 h to assess low-density lipoprotein (LDL) uptake. Samples were measured on a BD FACS Canto II flow cytometer (Becton–Dickinson, Heidelberg, Germany). BD FACSDiva (Becton–Dickinson) and Flowing Software (Cell Imaging Core, Turku Centre for Biotechnology, Turku, Finland) were used to analyze the data.

### *Detection of immunoglobulin and T-cell receptor gene recombinations*

Genomic DNA was isolated from (1) hiPSC-PB, (2) PBMCs from healthy donor, and (3) human dermal neonatal fibroblasts (HDFn; Thermo Fisher Scientific) using DNeasy Blood & Tissue Kit (Qiagen, Hilden, Germany) according to the manufacturer's protocol. DNA concentration was determined spectrophotometrically (NanoDrop ND-1000; NanoDrop

Technologies, Wilmington, DE). Rearranged immunoglobulin (Ig) and T-cell receptor (TCR) genes were analyzed by polymerase chain reaction (PCR) assays developed by European BIOMED-2 collaborative study [39]. Sixty-three primers were used in seven multiplex PCR tubes to detect (1) complete VH-JH rearrangement of immunoglobulin heavy chain (IGH) gene (three tubes), (2) complete V $\beta$ -J $\beta$  rearrangement of TRB gene (two tubes), and (3) TRG gene rearrangements (two tubes).

The PCR cocktail, final volume 50  $\mu$ L, contained 100 ng of genomic DNA, 25 pmol of each primer, 1  $\times$  Green GoTaq<sup>®</sup> Reaction Buffer (Promega, Madison, WI), 0.2 mM dNTP, and 1–2 U of GoTaq G2 DNA Polymerase (Promega). PCR was performed in a DNA Engine (PTC-200) Peltier Thermal Cycler (Bio-Rad Laboratories, Hercules, CA) and the cycling conditions were preactivation at 95°C for 7 min, followed by 35 cycles of denaturation at 95°C for 30 s, annealing at 60°C for 30 s, and extension at 73°C for 30 s, and a final extension at 74°C for 7 min. The PCR products of Ig/TCR genes were ultraviolet-visualized on 2% ethidium bromide-stained agarose gel. The presence of the expected size product was checked based on a 100 bp DNA Ladder (New England Biolabs, Ipswich, MA).

### *Endothelial differentiation*

Our protocol for the endothelial differentiation of hiPSCs was adapted from a method published by Orlova et al. [40]. In brief, hiPSCs were differentiated on Matrigel in BPEL medium [41] supplemented with the following growth factors: 25 ng/mL Activin A, 30 ng/mL BMP4, 50 ng/mL VEGF165, and 1.5 mM CHIR99021, a small molecule inhibitor. On the 3rd and 7th days, the medium was replaced with BPEL medium supplemented with 50 ng/mL VEGF and 10 mM SB43152. On the 10th day, cells were harvested, analyzed using flow cytometry and immunomagnetically separated using CD31-Microbeads (Miltenyi Biotec). The differentiation procedure generated 10%–45% CD31-positive cells. After separation, hiPSC-derived ECs were cultured on fibronectin-coated dishes in EGM-2 supplemented with 50 ng/mL VEGF.

### *Tube formation assay*

A 96-well  $\mu$ -plate for angiogenesis (Ibidi, Planegg, Germany) was coated with 50  $\mu$ L/well of growth factor-reduced Geltrex<sup>™</sup> (Thermo Fisher Scientific) and incubated at 37°C for 1 h. Cells were seeded at density of 5,000 cells/well in EGM-2 supplemented with 50 ng/mL VEGF and incubated in a 37°C incubator with a 5% CO<sub>2</sub> atmosphere for 24 h to allow tubes to form.

The number of complete rings formed during tube formation assay (TFA) was used to quantify the capability of ECs to form tubes. To count the number of rings in each well, we applied the following procedure. First, we subsampled the original images by a factor of four to reduce the size of images and still have the analyzed structures (rings) in a sufficient detail. The subsampling also reduced the noise in images, and therefore no further noise suppression was needed. Second, we calculated local standard deviation of intensity pixels in windows of size 3  $\times$  3 because the cells as well as their connections had much larger standard deviation from the local mean intensity than the background. It helped us to use a

single threshold to segment pixels belonging to cells and their connections. We used a minimum error method to set the appropriate threshold [42]. To remove small background as well as foreground structures in the segmented images, we applied the alternating sequential filter based on area closings and openings [43]. To count the number of rings we calculated the number of salient maxima of the Euclidian distance transform. As the salient maxima, we considered all maxima with a distance smaller than 200 pixels from the segmented structures (cells and their connections). It means that only rings with a radius smaller than  $\sim 400 \mu\text{m}$  were counted. The centers of the detected rings are visualized by the black cross.

### *Chemotaxis migration assay*

The cells were grown in Millicell<sup>®</sup> hanging cell culture inserts (Merck Millipore, Billerica, MA) in 24-well plates. hiPSC-derived ECs, HUVECs, and HSVECs were seeded onto the inside of the insert in EGM-2 without VEGF at density of  $2.5 \times 10^5$  cells per insert. Control HDFn were seeded in Fibroblast medium (DMEM medium, supplemented with 20% FBS, 2 mM L-glutamine, and 100  $\mu\text{M}$  nonessential amino acids; all from Life Technologies). Basolateral side was filled with EGM-2 or fibroblast medium containing 50 ng/mL VEGF. Cells were incubated in a 37°C incubator with a 5% CO<sub>2</sub> atmosphere for 18 h to allow the cells to migrate through the membrane. Cells on inserts were fixed with 4% paraformaldehyde (Sigma-Aldrich), permeabilized with 100% methanol (Lach-Ner, Neratovice, Czech Republic), and stained with 20 $\times$  diluted Giemsa stain (Sigma-Aldrich). Inner side of the insert was scraped with cotton swab and only cells on the outer side were counted under the microscope. For each cell culture insert, three representative images were counted. Each cell line was grown in three independent inserts.

### *Karyotype analysis*

Karyotype analyses were performed by Cytogenetic Laboratory Brno (Cytogenetická Laboratoř Brno, s.r.o., Brno, Czech Republic). In brief, hiPSCs at passage 16 or higher were grown to  $\sim 90\%$  confluence and exposed to 10  $\mu\text{g}/\text{mL}$  colcemid for 1 h. Harvested cells were exposed to a hypotonic solution (culture media diluted with deionized water at a 1:3 ratio) and fixed four times with methanol/acetic acid (3:1). Cells were then dropped onto glass slide and incubated at room temperature overnight. For Giemsa-banding, glass slides were incubated at 95°C for 10 min, washed with Sorensen's phosphate buffer at 50°C, and stained with Wright's stain for 1.5 min. After washing, the karyotype was determined by microscopic examination. Fifty mitosis events per sample were analyzed using "LUCIA Cytogenetics" software (Laboratory Imaging, Prague, Czech Republic).

### *DSB visualization by quantifying $\gamma\text{H2AX}$ foci and analyzing images*

Cells were first seeded onto microscope slides coated with Matrigel or gelatin in four-well plates to analyze the number of  $\gamma\text{H2AX}$  foci in G1 phase of the cell cycle. Four hours before fixation, a nucleoside analog of thymidine, EdU (5-ethynyl-2'-deoxyuridine; Thermo Fisher Scientific), was

added at a final concentration of 10  $\mu\text{M}$  to visualize cells in S/G2 phase of the cell cycle.

The cells were fixed with 4% paraformaldehyde and permeabilized with 0.2% Triton X-100. An overnight incubation with a primary antibody against  $\gamma\text{H2AX}$  (BioLegend, San Diego, CA) was followed by a 1 h incubation with a secondary antibody conjugated with Alexa Fluor 555 (Cell Signaling Technology). Samples were stained with the Click-iT<sup>®</sup> EdU Alexa Fluor<sup>®</sup> 488 Imaging Kit (Thermo Fisher Scientific) to visualize EdU, according to the manufacturer's instructions. Finally, the nuclei were stained with Hoechst dye. Fluorescent signals were detected using the Zeiss Axiovert 200M system (Carl Zeiss, Oberkochen, Germany). Images were captured using a CoolSNAP HQ2 CCD camera in the wide-field mode (Photometrics, Tucson, AZ) at  $-30^\circ\text{C}$ . Images of thirty slices at 0.3  $\mu\text{m}$  intervals were acquired in each field at a resolution of  $1,392 \times 1,040$  pixels. The pixel size of the images was  $124 \times 124 \text{ nm}$ .

The open-source software Acquarium [44] was used to acquire and analyze the images (<http://cbia.fi.muni.cz/projects/acquarium.html>), as previously described in detail [35]. In brief, the nucleus of each cell, which was stained with Hoechst dye, was automatically recognized and defined the area, in which we counted  $\gamma\text{H2AX}$  foci and assessed the intensity of the EdU signal. We used the eMax algorithm developed by Štěpka et al. to identify the  $\gamma\text{H2AX}$  foci [45]. The EdU signal was quantified based on the total intensity calculated in the nucleus. The threshold for the separation of EdU-negative (G1) and EdU-positive (S/G2) cells was computed in MATLAB (Mathworks, Natick, MA) using the Otsu method.

### *Teratoma formation*

The in vivo differentiation experiments were performed in duplicate for each hiPSC line. Six NOD SCID GAMMA mice were injected (three intramuscularly and three subcutaneously), and all mice developed teratomas after  $\sim 8$  weeks. In brief, hiPSCs were grown to near confluency on 6 cm Petri dishes and harvested with 0.5 mM EDTA. Cells were washed with PBS and resuspended in 40  $\mu\text{L}$  of cold PBS. An equal volume (40  $\mu\text{L}$ ) of Matrigel was added. The suspension was maintained on ice until it was injected into a mouse. The histological analysis of the teratomas was performed by Dr. Eva Mecova from the Department of Histology and Embryology, Masaryk University Brno.

### *Statistical analysis*

Data sets were compared using Student's *t*-test or the Mann-Whitney test.  $P < 0.05$  was considered statistically significant.

## **Results**

### *Generation of hiPSCs*

This study was performed on human cells that originated from the peripheral blood and endothelial tissue. PBMCs and HSVECs were isolated from adult tissue donors, whereas HUVECs represents a neonatal cell type. PBMCs, HUVECs, and HSVECs were reprogrammed into hiPSCs using episomal vectors [37]. Figure 1A illustrates the timeline of the



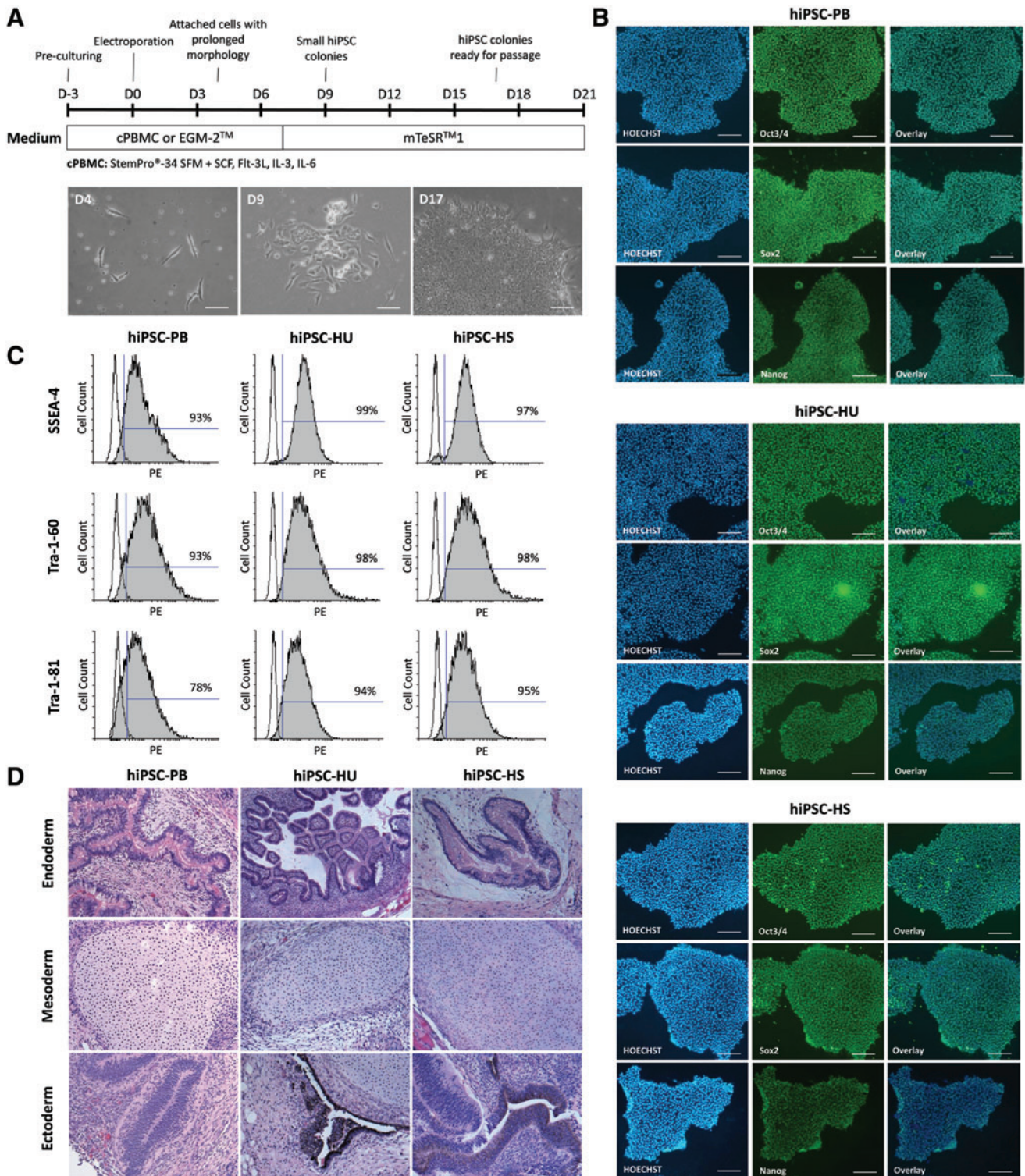


**FIG. 1.** hiPSC reprogramming and characterization. **(A)** Experimental timeline for the reprogramming of PBMCs and ECs into hiPSCs. Cell morphology observed during the reprogramming of PBMCs at days 4, 9, and 17 (scale bar = 100  $\mu$ m). **(B)** Immunofluorescence staining for the pluripotency markers Oct3/4, Sox2, and Nanog in hiPSCs (scale bar = 200  $\mu$ m). **(C)** Flow cytometry-based detection of the pluripotency markers SSEA-4, Tra-1-60, and Tra-1-81 in hiPSCs. **(D)** Teratoma formation in immunodeficient mice after transplantation of hiPSCs; teratomas contained tissues from all three germ layers. ECs, endothelial cells; hiPSC, human induced pluripotent stem cell; PBMCs, peripheral blood mononuclear cells. Color images are available online at [www.libepub.com/scd](http://www.libepub.com/scd)

reprogramming process, including the appropriate media for each cell type. The first attached cells with an elongated morphology were observed on day 4 after transfection. Small hiPSC colonies developed from these cells at approximately day 9. More than 15 hiPSC colonies emerged in each well on day 17, and these clones were mechanically passaged. At least 10 clones from each cell type were expanded and stored in liquid nitrogen.

The pluripotency of the generated hiPSC lines—hiPSC-PB, hiPSC-HU, and hiPSC-HS—was characterized. These hiPSCs displayed a typical hESC-like morphology and expressed the pluripotency markers Oct3/4, Sox2 and Nanog (Fig. 1B). Flow cytometry confirmed the expression of the surface pluripotency markers SSEA-4, Tra-1-60, and Tra-1-81 (Fig. 1C). In vivo teratoma formation revealed cell types representative of the three germ layers (Fig. 1D). To reveal which specific sub-population of PBMCs was reprogrammed, we performed PCR assays with seven multiplex PCR tubes (Fig. 2). No rearrangements in IGH gene (B lymphocytes), TRB gene, or TRG gene (T lymphocytes) were detected, suggesting that nonlymphoid mononuclear cell fraction was reprogrammed. The hiPSC-PB line therefore arose either from hematopoietic progenitor cell or from the monocyte fraction.

All the characterization methods confirmed that PBMCs, HUVECs, and HSVECs were reprogrammed into pluripotent cells that closely resembled hESCs.

*Endothelial differentiation of hiPSCs*

The main goal of our research was to compare ECs that had differentiated from hiPSCs with somatic ECs isolated from human donors and to prove that these cells are closely related in terms of their phenotype profiles and functionality. Three hiPSC lines, hiPSC-PB, hiPSC-HU, and hiPSC-HS, were differentiated in vitro using a previously published protocol [40], and the derived ECs were purified using CD31<sup>+</sup> microbeads.

The isolated ECs displayed an endothelial morphology and expressed typical endothelial surface markers within at least four passages following isolation (Fig. 3A). The phenotype profile of hiPSC-derived ECs generally resembled the control EC types, HUVECs and HSVECs, based on the expression of the endothelial surface markers CD31 and CD144. Specifically, as visualized in the graph shown in Fig. 3B, the percentage of the CD31-positive cells among hiPSC-derived ECs ranged from 84% to 95%, whereas their somatic EC counterparts, HUVECs and HSVECs, averaged more than 98% CD31-positive cells. Between 84% and 94% of hiPSC-ECs expressed CD144, whereas ~100% of HUVECs and HSVECs expressed CD144. For the markers CD34 and KDR, we observed high expression in the EC populations that had differentiated from hiPSCs, in contrast to the HUVEC and HSVEC controls. Approximately 81%, 95%, and 67% of

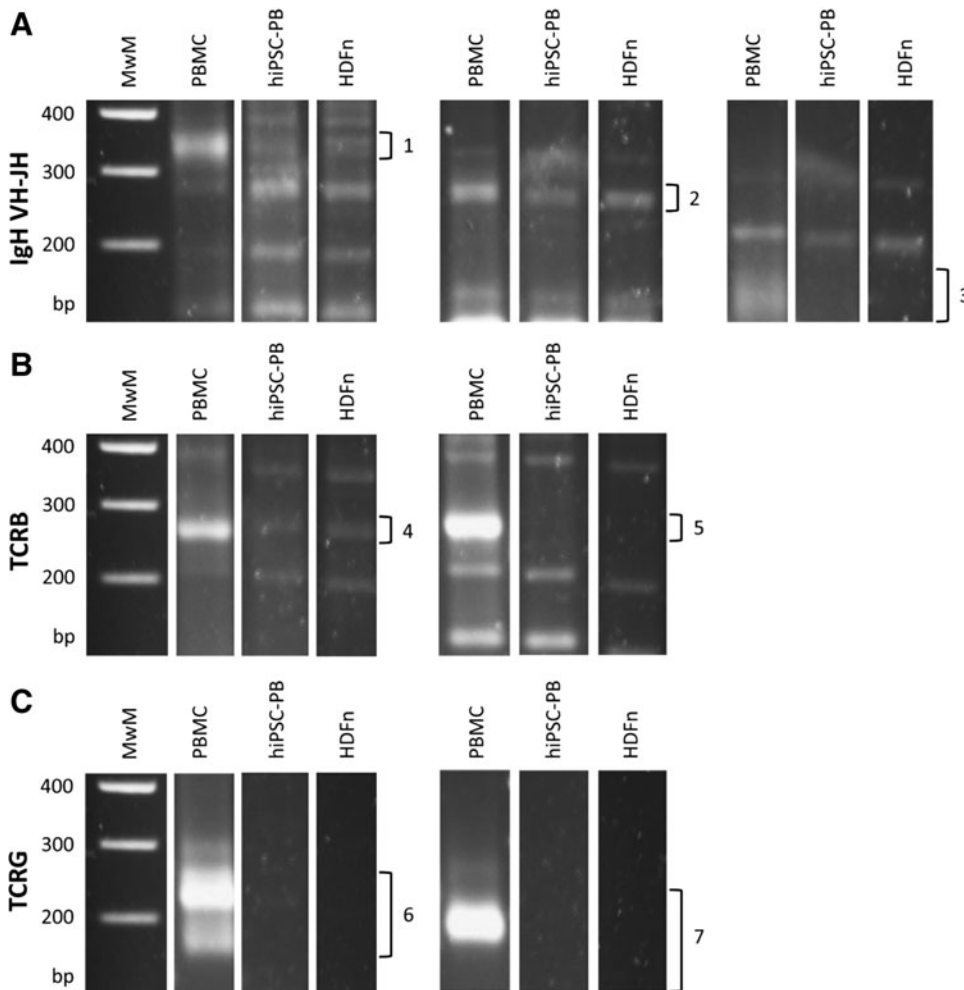


**FIG. 2.** Detection of Ig and TCR gene recombinations in hiPSC-PB. Genomic DNA from PBMCs is provided as a positive control, while fibroblast line (HDFn) serves as a negative control. Sixty-three primers were used in seven multiplex PCR tubes. (A) Complete VH-JH rearrangement of IGH gene. Three tubes were used with valid sizes of amplicon (1) 310–360 bp, (2) 250–295 bp, and (3) 100–170 bp. (B) Complete Vβ-Jβ rearrangement of TRB gene. Two tubes were used with valid sizes (4) 240–285 bp and (5) 240–285 bp. (C) TRG gene rearrangements. Two tubes were used with valid sizes (6) 145–255 bp and (7) 80–220 bp. MwM, molecular weight marker. HDFn, human dermal neonatal fibroblast; hiPSC-PB, hiPSC derived from PBMCs; Ig, immunoglobulin; PCR, polymerase chain reaction; TCR, T-cell receptor.

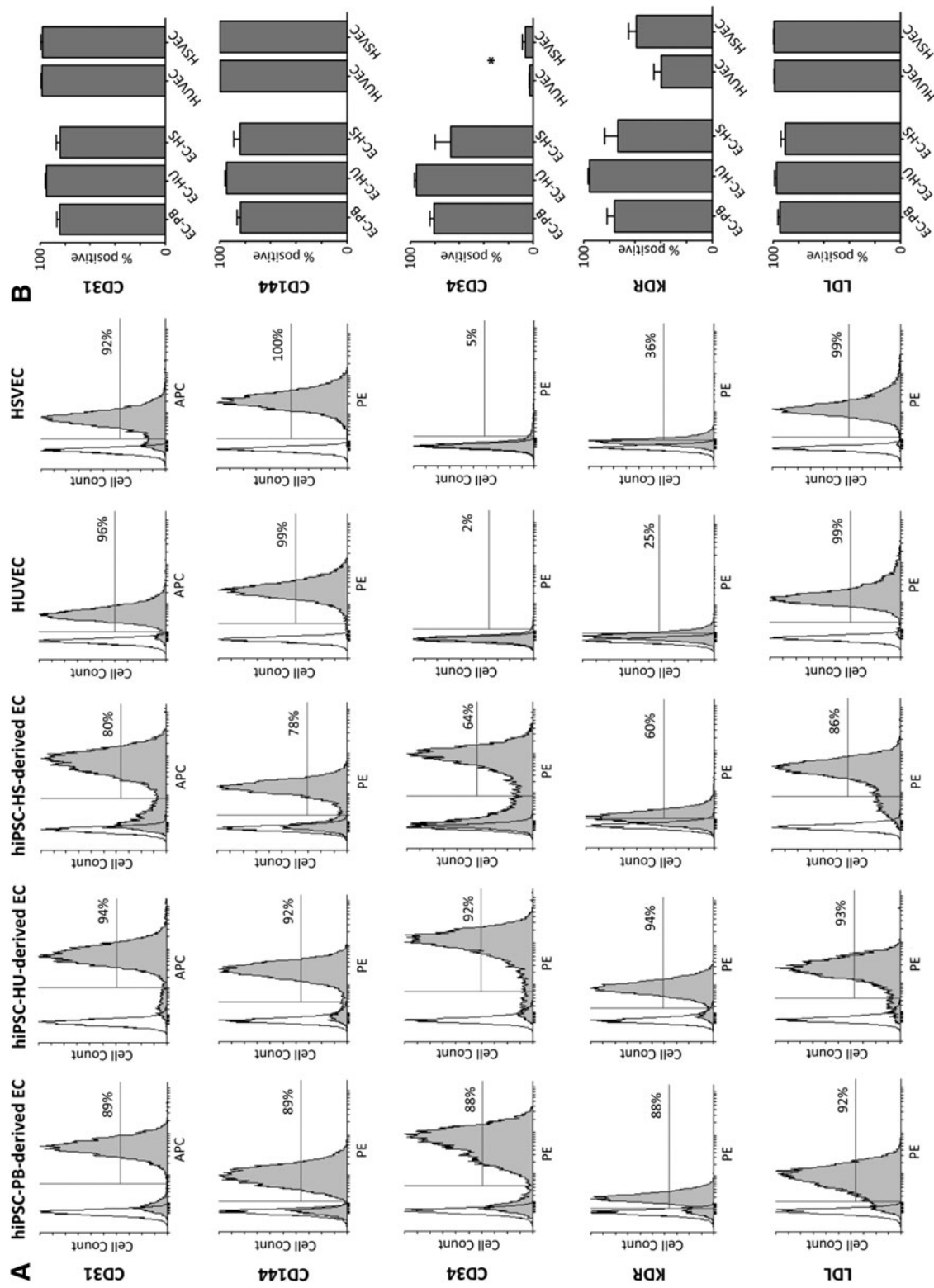


**FIG. 3.** Flow cytometry-based analysis of hiPSC-derived ECs and the EC controls. (A) Representative histograms showing the positivity for the cell surface markers CD31, CD144, CD34, KDR, and LDL in ECs derived from hiPSCs-PB, hiPSC-HU, and hiPSC-HS complemented with HUVECs and HSVECs. (B) Percentage of cells positive for each endothelial marker. The mean value was calculated from at least three independent differentiations of each hiPSC line ( $\pm$ SEM). The *asterisk* indicates a statistically significant ( $P < 0.05$ ) difference in percentage of positive hiPSCs-derived ECs compared with their EC counterparts, as detected using Student's *t*-test. hiPSC-HS, HSVEC-derived hiPSCs; hiPSC-HU, HUVEC-derived hiPSCs; HSVECs, human saphenous vein endothelial cells; HUVECs, human umbilical vein endothelial cells; KDR, kinase insert domain receptor; LDL, low-density lipoprotein; SEM, standard error of the mean.



EC-PB, EC-HU, and EC-HS expressed CD34, respectively, but <6% of their somatic EC counterparts were CD34-positive. A similar trend was observed for KDR: 76%, 95%, and 73% of hiPSC-derived ECs were positive compared with 40% and 59% of HUVECs and HSVECs, respectively.

Three elementary tests were performed to verify the functional properties of the ECs—(1) an LDL uptake assay, (2) a TFA, and (3) a chemotaxis migration assay. ECs derived from all three hiPSC lines displayed increased LDL uptake (Fig. 3A, B). More than 90% of cells in all measured EC samples were LDL-positive 4 h after the administration of the substance. Our hiPSC-ECs also formed tubes of the similar quality as the control ECs, HUVECs and HSVECs (Fig. 4A, B). The number of complete rings formed during the TFA averaged between 29 and 47 for hiPSC-derived ECs. Mean number of rings for HUVEC and HSVEC were 42 and 29, respectively. No rings were formed in HDFn sample. Finally, chemotaxis migration assay was performed to show the function of our hiPSC-derived ECs. Figure 4C and D illustrate that hiPSC-derived ECs are attracted by VEGF in the similar manner (between 268 and 373 cells per

one field of view) as HUVEC and HSVEC (363 and 344, respectively). Substantially less migrating cells were observed in control fibroblast sample (98 HDFn cells).

Based on these results, the directed in vitro differentiation of hiPSCs produced ECs that resembled HUVECs and HSVECs.

*Reprogramming and differentiation affect the cell cycle speed and DSB number*

Cellular reprogramming introduces serious changes into the genome and alters the cell fate. If hiPSC-derived cells are used in the clinic, their genomic stability must be monitored. Therefore, we next focused on detecting possible genomic abnormalities in our cells.

We analyzed the cell cycle speed, DSB numbers, and karyotypes. The number of  $\gamma$ H2AX foci, a measure of DSB, was counted in (1) hiPSCs derived from PBMC, HUVEC, and HSVEC somatic founders, (2) ECs differentiated from all three hiPSCs lines, and finally (3) control somatic ECs (HUVECs and HSVECs). The numbers of  $\gamma$ H2AX foci

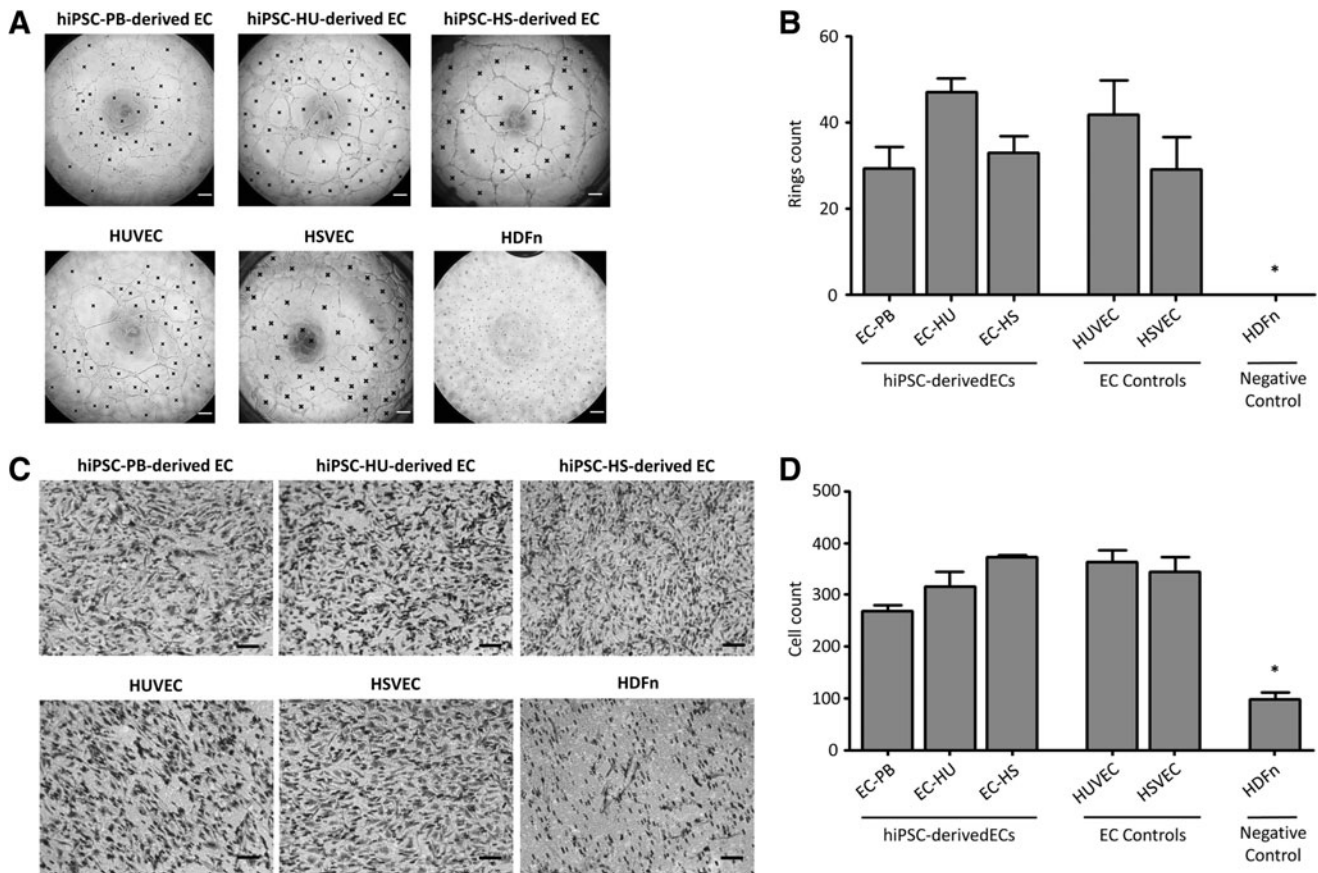


**FIG. 4.** Functional characterization of ECs derived from hiPSC-PB, hiPSC-HU, and hiPSC-HS. HUVEC and HSVEC serve as positive controls, while HDFn are provided as negative controls. (A) Tube formation assay. The number of complete rings was assessed by image analysis described in Materials and Methods section and labeled by *black cross*. Scale bar = 200  $\mu$ m. (B) Quantification of the tube formation assay. Each *column* indicates mean number of complete rings counted in three independent wells of 96-well plate ( $\pm$ SEM). *Asterisk* indicates statistically significant ( $P < 0.05$ ) difference in the HDFn ring count compared with the ECs ring counts, as detected using Student's *t*-test. (C) Chemotaxis migration assay. Only the cells on the outer side of the membrane which were attracted by VEGF (50 ng/mL) are shown. Scale bar = 100  $\mu$ m. (D) Quantification of the chemotaxis migration assay. Each *column* indicates mean number of cells counted in three independent cell culture inserts ( $\pm$ SEM). For each insert, three images were manually counted. *Asterisk* indicates statistically significant ( $P < 0.05$ ) difference in the HDFn cell count compared with the ECs cell counts, as detected using Student's *t*-test.

depend on the cell cycle phase, as substantially more foci are observed in the nuclei of cells in S/G2 phases than in cells in G1 phase due to the presence of replication-related DSBs. In this study, we compared somatic ECs with PSCs, cell types that differ in the lengths of their cell cycle phases. We used a highly sensitive method that was previously published by our team to obtain the most precise results [35].

Individual cells were first separated according to their actual cell cycle phase by labeling newly synthesized DNA with EdU. The EdU signal strength in each cell was plotted on a histogram, which allowed us to calculate the threshold for the number of cells in G1 phase as described in the Materials and Methods section. Figure 5A illustrates the distribution of EdU-negative (G1 phase) cells among samples. Reprogramming into pluripotent cells speeds up the cell cycle, as manifested by the decrease in the number of cells in G1 phase in all hiPSC lines. In somatic EC controls, the percentages of HUVECs and HSVECs in G1 phase were 67% and 81%, respectively, and decreased to 52%, 59%, and 68% for hiPSC-PB, hiPSC-HU, and hiPSC HS, respectively. As expected, the differentiation of hiPSCs into

ECs had the opposite effect and slowed the cell cycle again. Approximately 89% of ECs derived from hiPSC-PB, 80% of ECs derived from hiPSCs-HU, and 86% of ECs derived from hiPSC-HS were in G1 phase. Only the EdU-negative groups (G1 phase) were used for the subsequent analysis to exclude replication-related DSBs (S/G2 phase).

The numbers of  $\gamma$ H2AX foci were counted in cells in G1 phase to determine whether the process of reprogramming to pluripotent cells and subsequent endothelial differentiation influenced the numbers of DSBs. As shown in Fig. 5B, substantially larger numbers of  $\gamma$ H2AX foci were observed in the EdU-negative groups of hiPSCs lines than in all ECs, regardless of whether original somatic ECs or ECs derived from hiPSCs were analyzed. Specifically, in hiPSCs, the median numbers of foci per cell were 6, 7, and 6 for hiPSC-PB, hiPSC-HU, and hiPSC-HS, respectively. The median number of  $\gamma$ H2AX foci per cell in ECs differentiated from these hiPSCs decreased to 1 for all samples. The numbers of foci in hiPSC-derived ECs more closely resembled control ECs, in which no foci were detected in each cell.

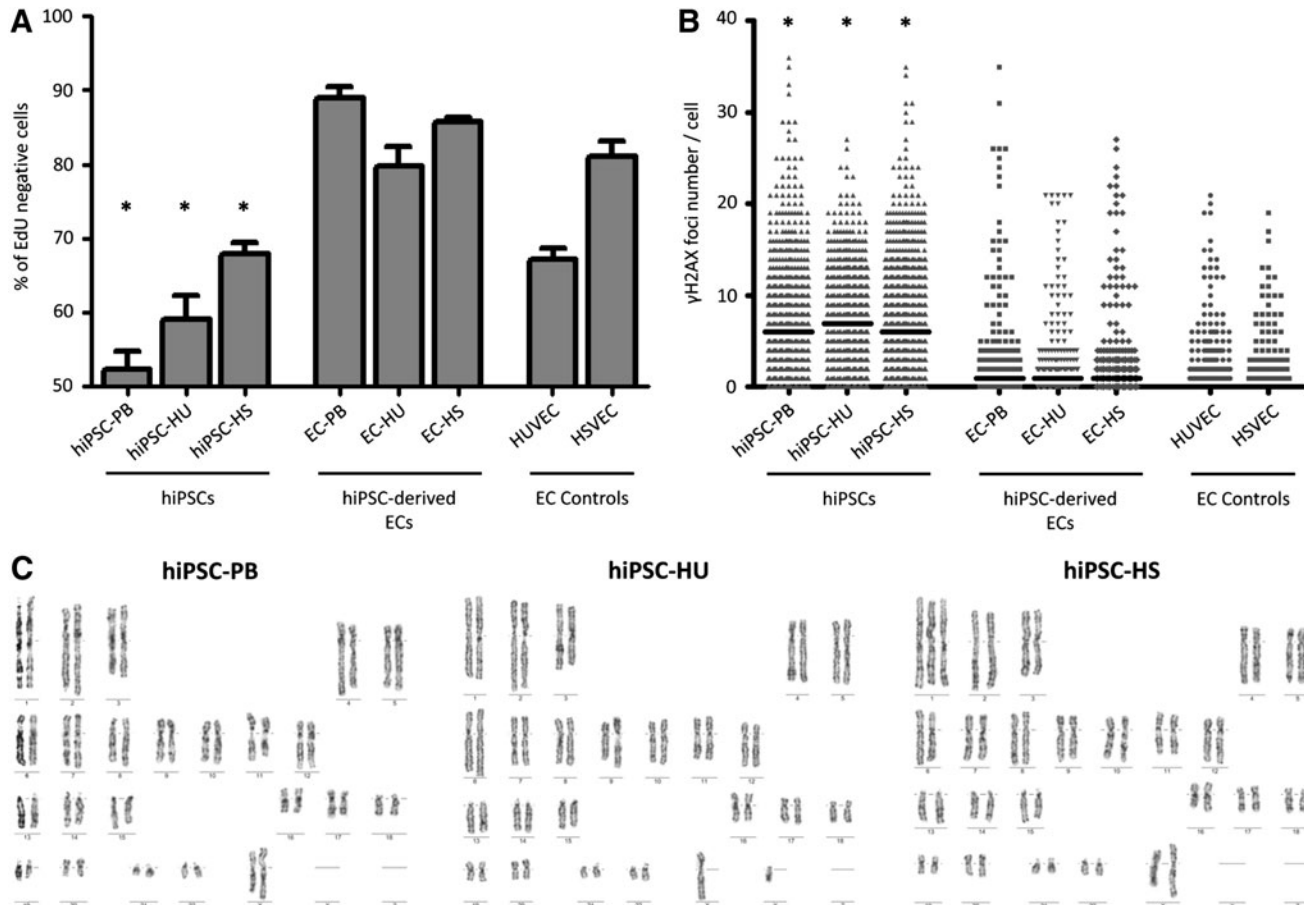


**FIG. 5.** Cell cycle speed and genome stability during the reprogramming and differentiation processes. **(A)** Percentage of EdU-negative (G1 phase) cells among hiPSCs, hiPSC-derived ECs, and EC controls. Mean value ( $\pm$ SEM;  $n=3$ ). Asterisks indicate statistically significant ( $P<0.05$ ) decreases in the percentages of hiPSCs in G1 phase compared with their EC counterparts, as detected using Student's *t*-test. **(B)** Number of  $\gamma$ H2AX foci per cell in hiPSCs, hiPSC-derived ECs and EC controls. The bar represents the median. Asterisks indicate statistically significant ( $P<0.05$ ) differences between hiPSCs and ECs, as confirmed by the Mann-Whitney test. **(C)** Cytogenetic data from hiPSC lines. Approximately 100% of cells possess a normal karyotype in hiPSC-PB and hiPSC-HU lines (passages 27 and 16, respectively). Representative aneuploid karyotype detected in 80% of cells in the hiPSC-HS line, in which a gain of chromosome 1 was observed (passage 17). EdU, 5-ethynyl-2'-deoxyuridine;  $\gamma$ H2AX, phosphorylated histone H2AX.

Finally, we performed a karyotype analysis of all three hiPSC lines to determine whether a faster cell cycle and larger number of DSBs in hiPSCs led to chromosomal abnormalities (Fig. 5C). A normal karyotype was observed in the hiPSC-PB (46, xx) and hiPSC-HU (46, xy) cell lines. A heterogeneous cell population was detected in the hiPSC-HS line, as 80% of the cells gained chromosome 1 (47, xx). Thus, the genome stability of hiPSCs is challenged during *in vitro* culture and should be closely monitored.

## Discussion

ECs are valuable tools in regenerative medicine. Their use in the *de novo* regeneration of injured veins and the lining of vascular grafts is promising. However, the sources of ECs are limited, and therefore, new methods for ECs production are being developed. In our study, we produced ECs from hiPSCs and compared them with ECs isolated from donors (HUVECs and HSVECs) to confirm that the derived ECs resembled natural ECs. The hiPSCs used in this project were generated from three somatic cell types. We focused on the most easily accessible tissue—peripheral blood—as well as hiPSCs derived from HUVECs and HSVECs.

PBMCs offer several advantages over cell types that are traditionally used for hiPSC generation, such as dermal fibroblasts or, less often, ECs. Surgical removal of the skin tissue is painful and leaves a scar, which discourages potential donors. Fibroblasts or ECs are usually collected from donors during a planned surgery, such as plastic surgery or varicose vein surgery, which limits the opportunities to obtain tissue sample from patients with specific diseases, such as rare genetic disorders. In contrast, the routine collection of a few milliliters of blood is a minimally invasive procedure. The existence of blood banks is another argument favoring blood cells as a source for hiPSC production. The total amount of time needed for the derivation of the primary cell line is an important factor. A few weeks are needed to expand cells from skin tissue *in vitro*, whereas only 3 days of preculture are sufficient for PBMCs before reprogramming (Fig. 1A). The establishment of our HSVEC lines from vein samples usually requires between 2 and 3 weeks.

Several protocols for the expansion and reprogramming of PBMCs have been published [25–29]. In these studies, hiPSCs were reprogrammed using different vectors under different culture conditions. One of the most important issues is the composition of medium used for preculturing PBMCs before reprogramming and during the first days after reprogramming. StemPro-34 medium influences the ratio of particular blood cell types in the sample and induces the proliferation of hematopoietic progenitor cells to a greater extent than terminally differentiated lymphocytes. Various combinations of cytokine cocktails used to support the growth of hematopoietic progenitors have been proposed, but all include one or more of the following nine growth factors: SCF, Flt-3L, IL-6, IL-3, IL-1, erythropoietin (EPO), thrombopoietin (TPO), granulocyte colony-stimulating factor (G-CSF), and granulocyte-macrophage CSF (GM-CSF) (reviewed in Heike and Nakahata [46]).

In our study, we enriched the StemPro-34 medium with a combination of the growth factors SCF, Flt-3L, IL-3, and IL-6, which was reported to significantly increase the percentage of human hematopoietic progenitor cells expressing the CD34 surface marker [31] and should facilitate the reprogramming

process of PBMCs. Similar medium, with addition of TPO, was used for pre-reprogramming expansion of CD34<sup>+</sup> cells by Mack et al. [30].

Our PCR results excluded DNA rearrangements associated with T- or B-lymphocytes in hiPSC-PB cell line, which implies that hematopoietic progenitors were reprogrammed without the need for time-consuming isolation process of CD34<sup>+</sup> cells from peripheral blood or mobilizing the blood as reported by Loh et al. [24]. Although we cannot exclude the possibility that monocytes were reprogrammed, it is unlikely because of difficult *ex vivo* expansion of this cell type [47,48]. It is of note that our hiPSC-PB contains unmodified DNA without gene recombinations introduced during lymphoid maturation.

Two EC types, HUVECs and HSVECs, were used in the study as EC controls and to complement PBMCs for hiPSC derivation. HUVECs were purchased from Thermo Fisher Scientific and HSVECs were isolated from the saphenous vein of an adult donor. The protocol used to isolate HSVECs in this study is simple and effective. Enzymatic digestion with collagenase II did not result in contamination with other cell types, and a pure population of primary HSVECs was successfully characterized using both surface markers and a functional TFA. Primary ECs have a relatively short life-span *in vitro*, displaying signs of dedifferentiation into fibroblasts and senescence after a few passages [49]. We were able to expand HUVECs and HSVECs for up to ~10 passages. Although our hiPSC-ECs did not exceed 10 passages in the majority of differentiations, hiPSC-derived ECs offer a constant and theoretically unlimited source of uniform cells for vascular grafts and *in vitro* studies. Robust protocols for the differentiation of hiPSCs into ECs have been recently published [20,21,40].

In the present study, we did not detect significant differences in the quality of hiPSCs or hiPSC-derived ECs between the three tested hiPSC lines derived from PBMCs, HUVECs, and HSVECs. All hiPSC lines produced hiPSC-derived ECs that were almost indistinguishable from each other and from the original ECs, based on their expression of the endothelial markers CD31 and CD144, LDL uptake, ability to form tubes, and chemotaxis migration.

Unlike the original ECs, hiPSC-derived ECs expressed higher levels of the endothelial progenitor markers CD34 and KDR. A substantial effort has attempted by other groups to identify and isolate EPCs that are capable of producing functional ECs (reviewed in Pelosi et al. [50]). Physiologically, EPCs are present in the human body as circulating cells that share common endothelial markers with mature ECs, such as CD31, but differ in the expression of certain cell surface antigens, such as CD34 and KDR [51–53]. EPCs are often divided into two subgroups, termed early- and late-outgrowth EPCs [54,55]. Late-outgrowth EPCs, unlike early-outgrowth EPCs, contribute to blood vessels formation and repairation by direct incorporation into their endothelial lining [56,57]. Based on phenotypical profile (CD31<sup>+</sup>CD144<sup>+</sup>CD34<sup>+</sup>KDR<sup>+</sup>) and ability to form tubes [56–58], our hiPSC-derived cells resemble late outgrowth EPCs.

Genomic stability is a key issue in the use of hiPSC-derived cells in the clinic. For this reason, we studied the effect of *in vitro* cellular reprogramming and endothelial differentiation on the cell cycle speed and number of DSBs. In addition, a karyotype analysis of three tested hiPSC lines was performed.

The analysis of the cell cycle speed revealed differences between samples. The lowest percentage of cells in G1

phase was observed in hiPSCs, suggesting that these cells have a higher proliferation rate than their differentiated counterparts (hiPSC-derived ECs and ECs). This result is consistent with previously published data [59–62]. The number of DSBs observed in G1 phase is substantially increased in S/G2 phases as a consequence of replication stress [63–67]. Therefore, we used methodology that had been previously published by our team to reliably compare DSB counts visualized by  $\gamma$ H2AX foci between samples with different cell cycle speeds [35]. Fluorescence microscopy enables us to analyze the number of  $\gamma$ H2AX foci in each single cell, assign the cell cycle phase to that particular cell and only include G1 phase cells in the DSB analysis. Greater numbers of  $\gamma$ H2AX foci were recorded for the hiPSC group compared to hiPSC-derived ECs and primary ECs, suggesting that the reprogramming process increases the number of DSBs, but differentiation restores DSBs to a number typically observed in somatic cells.

High DSB counts in pluripotent cells may increase the risk of acquiring chromosomal or subchromosomal abnormalities and challenge the overall genome stability of the cells. According to Laurent et al., hESC and hiPSC cells contain a greater frequency of subchromosomal copy number variations than somatic cells or tissues [33]. In our study, hiPSC lines hiPSC-PB and hiPSC-HU displayed a normal karyotype. However, the hiPSC-HS culture was mosaic and contained two populations of cells, one with a normal karyotype and one with an abnormal karyotype, characterized by a gain of chromosome 1. Trisomy of chromosome 1 is a common abnormality detected in PSCs. Mayshar et al. identified an extra copy of chromosome 1 in several tested hiPSC lines, but no corresponding aneuploidy was detected in the somatic cells [68]. Amps et al. observed mosaic hESC lines at an early passage, with extra copies of chromosomes 1, 12, 17, 20, or X [69–72].

The chromosomal abnormality we observed in the subset of hiPSCs derived from HSVEC probably results from the clonal selection during passaging and adaptation to culture conditions. Prolonged in vitro culturing of PSCs is associated with karyotypic abnormalities [32,33] and karyotype analysis is a crucial test for selection of hiPSC clones [73]. Structural alteration, loss, or gain of a particular chromosome must lead to immediate exclusion of the clone or its derivative from any possible clinical application. Our results confirm that prolonged in vitro culturing of hiPSCs should be avoided and the time in culture before differentiation should be kept on necessary minimum.

Based on our data, PBMCs may serve as a safe and reliable source for artificial EC production for clinical purposes. hiPSC-derived ECs are fully functional and comparable with EC controls. In this protocol, cells pass through a pluripotent state, during which the number of DSBs increases and genome stability is challenged. Even if the number of DSBs is reversed upon endothelial differentiation, close monitoring of a normal karyotype is crucial for the possible clinical application of hiPSC-derived ECs.

## Acknowledgments

This study was generously supported by the Grant Agency of the Czech Republic (302/12/G157), by the Czech Health Research Council (16-31501A), and by the European Regional Development Fund (FNUSA-ICRC, no. CZ.1.05/1.1.00/02.0123).

## Author Disclosure Statement

No competing financial interests exist.

## References

- Carmeliet P. (2000). Mechanisms of angiogenesis and arteriogenesis. *Nat Med* 6:389–395.
- Folkman J. (1995). Angiogenesis in cancer, vascular, rheumatoid and other disease. *Nat Med* 1:27–31.
- Cooke JP. (2003). Flow, NO, and atherogenesis. *Proc Natl Acad Sci U S A* 100:768–770.
- Huang L, C Perrault, J Coelho-Martins, C Hu, C Dulong, M Varna, J Liu, J Jin, C Soria, et al. (2013). Induction of acquired drug resistance in endothelial cells and its involvement in anticancer therapy. *J Hematol Oncol* 6:49.
- Folkman J. (2007). Angiogenesis: an organizing principle for drug discovery? *Nat Rev Drug Discov* 6:273–286.
- Herring M, S Baughman and J Glover. (1985). Endothelium develops on seeded human arterial prosthesis: a brief clinical note. *J Vasc Surg* 2:727–730.
- Herring M, A Gardner and J Glover. (1978). A single-staged technique for seeding vascular grafts with autogenous endothelium. *Surgery* 84:498–504.
- Chong MS, WK Ng and JK Chan. (2016). Concise review: endothelial progenitor cells in regenerative medicine: applications and challenges. *Stem Cells Transl Med* 5:530–538.
- Jaffe EA, RL Nachman, CG Becker and CR Minick. (1973). Culture of human endothelial cells derived from umbilical veins. Identification by morphologic and immunologic criteria. *J Clin Invest* 52:2745–2756.
- Watkins MT, JB Sharefkin, R Zajtchuk, TM Maciag, PA D'Amore, US Ryan, H Van Wart and NM Rich. (1984). Adult human saphenous vein endothelial cells: assessment of their reproductive capacity for use in endothelial seeding of vascular prostheses. *J Surg Res* 36:588–596.
- Kinoshita M, Y Fujita, M Katayama, R Baba, M Shibakawa, K Yoshikawa, N Katakami, Y Furukawa, T Tsukie, et al. (2012). Long-term clinical outcome after intramuscular transplantation of granulocyte colony stimulating factor-mobilized CD34 positive cells in patients with critical limb ischemia. *Atherosclerosis* 224:440–445.
- Barsheshet A, H Hod, M Shechter, O Sharabani-Yosef, E Rosenthal, IM Barbash, S Matetzky, R Tal, AG Bentancur, et al. (2008). The effects of external counter pulsation therapy on circulating endothelial progenitor cells in patients with angina pectoris. *Cardiology* 110:160–166.
- Baran Ç, S Durdu, K Dalva, Ç Zaim, A Dogan, G Ocakoglu, G Gürman, Ö Arslan and AR Akar. (2012). Effects of preoperative short term use of atorvastatin on endothelial progenitor cells after coronary surgery: a randomized, controlled trial. *Stem Cell Rev* 8:963–971.
- Wang ZZ, P Au, T Chen, Y Shao, LM Daheron, H Bai, M Arzigian, D Fukumura, RK Jain and DT Scadden. (2007). Endothelial cells derived from human embryonic stem cells form durable blood vessels in vivo. *Nat Biotechnol* 25:317–318.
- Kane NM, M Meloni, HL Spencer, MA Craig, R Strehl, G Milligan, MD Houslay, JC Mountford, C Emanuelli and AH Baker. (2010). Derivation of endothelial cells from human embryonic stem cells by directed differentiation: analysis of microRNA and angiogenesis in vitro and in vivo. *Arterioscler Thromb Vasc Biol* 30:1389–1397.
- Nourse MB, DE Halpin, M Scatena, DJ Mortisen, NL Tulloch, KD Hauch, B Torok-Storb, BD Ratner, L Pabon and CE Murry. (2010). VEGF induces differentiation of

- functional endothelium from human embryonic stem cells: implications for tissue engineering. *Arterioscler Thromb Vasc Biol* 30:80–89.
17. Rufaihah AJ, NF Huang, S Jamé, JC Lee, HN Nguyen, B Byers, A De, J Okogbaa, M Rollins, et al. (2011). Endothelial cells derived from human iPSCs increase capillary density and improve perfusion in a mouse model of peripheral arterial disease. *Arterioscler Thromb Vasc Biol* 31:e72–e79.
  18. White MP, AJ Rufaihah, L Liu, YT Ghebremariam, KN Ivey, JP Cooke and D Srivastava. (2013). Limited gene expression variation in human embryonic stem cell and induced pluripotent stem cell-derived endothelial cells. *Stem Cells* 31:92–103.
  19. Orlova VV, Y Drabsch, C Freund, S Petrus-Reurer, FE van den Hil, S Muenthaiong, PT Dijke and CL Mummery. (2014). Functionality of endothelial cells and pericytes from human pluripotent stem cells demonstrated in cultured vascular plexus and zebrafish xenografts. *Arterioscler Thromb Vasc Biol* 34:177–186.
  20. Patsch C, L Challet-Meylan, EC Thoma, E Urich, T Heckel, JF O’Sullivan, SJ Grainger, FG Kapp, L Sun, et al. (2015). Generation of vascular endothelial and smooth muscle cells from human pluripotent stem cells. *Nat Cell Biol* 17:994–1003.
  21. Sahara M, EM Hansson, O Wernet, KO Lui, D Später and KR Chien. (2014). Manipulation of a VEGF-Notch signaling circuit drives formation of functional vascular endothelial progenitors from human pluripotent stem cells. *Cell Res* 24:820–841.
  22. Takahashi K, K Tanabe, M Ohnuki, M Narita, T Ichisaka, K Tomoda and S Yamanaka. (2007). Induction of pluripotent stem cells from adult human fibroblasts by defined factors. *Cell* 131:861–872.
  23. Yu J, MA Vodyanik, K Smuga-Otto, J Antosiewicz-Bourget, JL Frane, S Tian, J Nie, GA Jonsdottir, V Ruotti, et al. (2007). Induced pluripotent stem cell lines derived from human somatic cells. *Science* 318:1917–1920.
  24. Loh YH, S Agarwal, IH Park, A Urbach, H Huo, GC Heffner, K Kim, JD Miller, K Ng and GQ Daley. (2009). Generation of induced pluripotent stem cells from human blood. *Blood* 113:5476–5479.
  25. Staerk J, MM Dawlaty, Q Gao, D Maetzel, J Hanna, CA Sommer, G Mostoslavsky and R Jaenisch. (2010). Reprogramming of human peripheral blood cells to induced pluripotent stem cells. *Cell Stem Cell* 7:20–24.
  26. Loh YH, O Hartung, H Li, C Guo, JM Sahalie, PD Manos, A Urbach, GC Heffner, M Grskovic, et al. (2010). Reprogramming of T cells from human peripheral blood. *Cell Stem Cell* 7:15–19.
  27. Okita K, T Yamakawa, Y Matsumura, Y Sato, N Amano, A Watanabe, N Goshima and S Yamanaka. (2013). An efficient nonviral method to generate integration-free human-induced pluripotent stem cells from cord blood and peripheral blood cells. *Stem Cells* 31:458–466.
  28. Chou BK, P Mali, X Huang, Z Ye, SN Dowey, LM Resar, C Zou, YA Zhang, J Tong and L Cheng. (2011). Efficient human iPS cell derivation by a non-integrating plasmid from blood cells with unique epigenetic and gene expression signatures. *Cell Res* 21:518–529.
  29. Li Y, T Liu, N Van Halm-Lutterodt, J Chen, Q Su and Y Hai. (2016). Reprogramming of blood cells into induced pluripotent stem cells as a new cell source for cartilage repair. *Stem Cell Res Ther* 7:31.
  30. Mack AA, S Kroboth, D Rajesh and WB Wang. (2011). Generation of induced pluripotent stem cells from CD34<sup>+</sup> cells across blood drawn from multiple donors with non-integrating episomal vectors. *PLoS One* 6:e27956.
  31. Shah AJ, EM Smogorzewska, C Hannum and GM Crooks. (1996). Flt3 ligand induces proliferation of quiescent human bone marrow CD34<sup>+</sup>CD38<sup>−</sup> cells and maintains progenitor cells in vitro. *Blood* 87:3563–3570.
  32. Taapken SM, BS Nisler, MA Newton, TL Sampsel-Barron, KA Leonhard, EM McIntire and KD Montgomery. (2011). Karyotypic abnormalities in human induced pluripotent stem cells and embryonic stem cells. *Nat Biotechnol* 29:313–314.
  33. Laurent LC, I Ulitsky, I Slavin, H Tran, A Schork, R Morey, C Lynch, JV Harness, S Lee, et al. (2011). Dynamic changes in the copy number of pluripotency and cell proliferation genes in human ESCs and iPSCs during reprogramming and time in culture. *Cell Stem Cell* 8:106–118.
  34. Shrivastav M, LP De Haro and JA Nickoloff. (2008). Regulation of DNA double-strand break repair pathway choice. *Cell Res* 18:134–147.
  35. Simara P, L Tesarova, D Rehakova, P Matula, S Stejskal, A Hampl and I Koutna. (2017). DNA double-strand breaks in hiPSC reprogramming and long-term in vitro culturing. *Stem Cell Res Ther* 8:73.
  36. Weissbein U, N Benvenisty and U Ben-David. (2014). Quality control: genome maintenance in pluripotent stem cells. *J Cell Biol* 204:153–163.
  37. Yu J, K Hu, K Smuga-Otto, S Tian, R Stewart, II Slukvin and JA Thomson. (2009). Human induced pluripotent stem cells free of vector and transgene sequences. *Science* 324:797–801.
  38. Šimara P, L Tesařová, S Padourová and I Koutná. (2014). Generation of human induced pluripotent stem cells using genome integrating or non-integrating methods. *Folia Biol (Praha)* 60 (Suppl. 1):85–89.
  39. van Dongen JJ, AW Langerak, M Brüggemann, PA Evans, M Hummel, FL Lavender, E Delabesse, F Davi, E Schuurung, et al. (2003). Design and standardization of PCR primers and protocols for detection of clonal immunoglobulin and T-cell receptor gene recombinations in suspect lymphoproliferations: report of the BIOMED-2 Concerted Action BMH4-CT98–3936. *Leukemia* 17:2257–2317.
  40. Orlova VV, FE van den Hil, S Petrus-Reurer, Y Drabsch, P Ten Dijke and CL Mummery. (2014). Generation, expansion and functional analysis of endothelial cells and pericytes derived from human pluripotent stem cells. *Nat Protoc* 9:1514–1531.
  41. Ng ES, R Davis, EG Stanley and AG Elefanty. (2008). A protocol describing the use of a recombinant protein-based, animal product-free medium (APEL) for human embryonic stem cell differentiation as spin embryoid bodies. *Nat Protoc* 3:768–776.
  42. Kittler J and J Illingworth. (1986). Minimum error thresholding. *Pattern Recognit* 19:41–47.
  43. Soille P. (2004). *Morphological Image Analysis*. New York, NY: Springer-Verlag.
  44. Matula P, M Maška, O Daněk, P Matula and M Kozubek. (2009). Acquarium: free software for acquisition and analysis of 3D images of cells in fluorescence microscopy. In: *6th IEEE International Symposium on Biomedical Imaging*. Boston, pp. 1138–1141.
  45. Štěpka K, P Matula, S Wörz, K Rohr and M Kozubek. (2015). Performance and sensitivity evaluation of 3D spot detection methods in confocal microscopy. *Cytometry A* 87:759–772.
  46. Heike T and T Nakahata. (2002). Ex vivo expansion of hematopoietic stem cells by cytokines. *Biochim Biophys Acta* 1592:313–321.



47. Kim Y, YA Rim, H Yi, N Park, SH Park and JH Ju. (2016). The generation of human induced pluripotent stem cells from blood cells: an efficient protocol using serial plating of reprogrammed cells by centrifugation. *Stem Cells Int* 2016:1329459.
48. Zhang XB. (2013). Cellular reprogramming of human peripheral blood cells. *Genomics Proteomics Bioinformatics* 11:264–274.
49. Scoumanne A, T Kalamati, J Moss, JT Powell, M Gosling and N Carey. (2002). Generation and characterisation of human saphenous vein endothelial cell lines. *Atherosclerosis* 160:59–67.
50. Pelosi E, G Castelli and U Testa. (2014). Endothelial progenitors. *Blood Cells Mol Dis* 52:186–194.
51. Asahara T, T Murohara, A Sullivan, M Silver, R van der Zee, T Li, B Witzenbichler, G Schatteman and JM Isner. (1997). Isolation of putative progenitor endothelial cells for angiogenesis. *Science* 275:964–967.
52. Peichev M, AJ Naiyer, D Pereira, Z Zhu, WJ Lane, M Williams, MC Oz, DJ Hicklin, L Witte, MA Moore and S Rafii. (2000). Expression of VEGFR-2 and AC133 by circulating human CD34(+) cells identifies a population of functional endothelial precursors. *Blood* 95:952–958.
53. de la Puente P, B Muz, F Azab and AK Azab. (2013). Cell trafficking of endothelial progenitor cells in tumor progression. *Clin Cancer Res* 19:3360–3368.
54. Hur J, CH Yoon, HS Kim, JH Choi, HJ Kang, KK Hwang, BH Oh, MM Lee and YB Park. (2004). Characterization of two types of endothelial progenitor cells and their different contributions to neovascularization. *Arterioscler Thromb Vasc Biol* 24:288–293.
55. Medina RJ, CL Barber, F Sabatier, F Dignat-George, JM Melero-Martin, K Khosrotehrani, O Ohneda, AM Randi, JKY Chan, et al. (2017). Endothelial progenitors: a consensus statement on nomenclature. *Stem Cells Transl Med* 6:1316–1320.
56. Minami Y, T Nakajima, M Ikutomi, T Morita, I Komuro, M Sata and M Sahara. (2015). Angiogenic potential of early and late outgrowth endothelial progenitor cells is dependent on the time of emergence. *Int J Cardiol* 186:305–314.
57. Mukai N, T Akahori, M Komaki, Q Li, T Kanayasu-Toyoda, A Ishii-Watabe, A Kobayashi, T Yamaguchi, M Abe, T Amagasa and I Morita. (2008). A comparison of the tube forming potentials of early and late endothelial progenitor cells. *Exp Cell Res* 314:430–440.
58. Cheng CC, SJ Chang, YN Chueh, TS Huang, PH Huang, SM Cheng, TN Tsai, JW Chen and HW Wang. (2013). Distinct angiogenesis roles and surface markers of early and late endothelial progenitor cells revealed by functional group analyses. *BMC Genomics* 14:182.
59. Stead E, J White, R Faast, S Conn, S Goldstone, J Rathjen, U Dhingra, P Rathjen, D Walker and S Dalton. (2002). Pluripotent cell division cycles are driven by ectopic Cdk2, cyclin A/E and E2F activities. *Oncogene* 21:8320–8333.
60. Becker KA, PN Ghule, JA Therrien, JB Lian, JL Stein, AJ van Wijnen and GS Stein. (2006). Self-renewal of human embryonic stem cells is supported by a shortened G1 cell cycle phase. *J Cell Physiol* 209:883–893.
61. Calder A, I Roth-Albin, S Bhatia, C Pilquil, JH Lee, M Bhatia, M Levadoux-Martin, J McNicol, J Russell, T Collins and JS Draper. (2013). Lengthened G1 phase indicates differentiation status in human embryonic stem cells. *Stem Cells Dev* 22:279–295.
62. Barta T, D Dolezalova, Z Holubcova and A Hampl. (2013). Cell cycle regulation in human embryonic stem cells: links to adaptation to cell culture. *Exp Biol Med* (Maywood) 238:271–275.
63. Adams BR, SE Golding, RR Rao and K Valerie. (2010). Dynamic dependence on ATR and ATM for double-strand break repair in human embryonic stem cells and neural descendants. *PLoS One* 5:e10001.
64. Huang X, T Tanaka, A Kurose, F Traganos and Z Darzynkiewicz. (2006). Constitutive histone H2AX phosphorylation on Ser-139 in cells untreated by genotoxic agents is cell-cycle phase specific and attenuated by scavenging reactive oxygen species. *Int J Oncol* 29:495–501.
65. MacPhail SH, JP Banáth, Y Yu, E Chu and PL Olive. (2003). Cell cycle-dependent expression of phosphorylated histone H2AX: reduced expression in unirradiated but not X-irradiated G1-phase cells. *Radiat Res* 159:759–767.
66. Suchánková J, S Kozubek, S Legartová, P Sehnalová, T Küntziger and E Bártová. (2015). Distinct kinetics of DNA repair protein accumulation at DNA lesions and cell cycle-dependent formation of  $\gamma$ H2AX- and NBS1-positive repair foci. *Biol Cell* 107:440–454.
67. Suzuki K, H Okada, M Yamauchi, Y Oka, S Kodama and M Watanabe. (2006). Qualitative and quantitative analysis of phosphorylated ATM foci induced by low-dose ionizing radiation. *Radiat Res* 165:499–504.
68. Maysar Y, U Ben-David, N Lavon, JC Biancotti, B Yakir, AT Clark, K Plath, WE Lowry and N Benvenisty. (2010). Identification and classification of chromosomal aberrations in human induced pluripotent stem cells. *Cell Stem Cell* 7:521–531.
69. Amps K, PW Andrews, G Anyfantis, L Armstrong, S Avery, H Baharv, J Baker, D Baker, MB Munoz, et al. (2011). Screening ethnically diverse human embryonic stem cells identifies a chromosome 20 minimal amplicon conferring growth advantage. *Nat Biotechnol* 29:1132–1144.
70. Baker DE, NJ Harrison, E Maltby, K Smith, HD Moore, PJ Shaw, PR Heath, H Holden and PW Andrews. (2007). Adaptation to culture of human embryonic stem cells and oncogenesis in vivo. *Nat Biotechnol* 25:207–215.
71. Draper JS, K Smith, P Gokhale, HD Moore, E Maltby, J Johnson, L Meisner, TP Zwaka, JA Thomson and PW Andrews. (2004). Recurrent gain of chromosomes 17q and 12 in cultured human embryonic stem cells. *Nat Biotechnol* 22:53–54.
72. Ben-David U, Y Maysar and N Benvenisty. (2011). Large-scale analysis reveals acquisition of lineage-specific chromosomal aberrations in human adult stem cells. *Cell Stem Cell* 9:97–102.
73. Mandai M, A Watanabe, Y Kurimoto, Y Hirami, C Morinaga, T Daimon, M Fujihara, H Akimaru, N Sakai, et al. (2017). Autologous induced stem-cell-derived retinal cells for macular degeneration. *N Engl J Med* 376:1038–1046.

Address correspondence to:

*Pavel Simara, PhD*

*Centre for Biomedical Image Analysis*

*Faculty of Informatics*

*Masaryk University*

*University Campus Bohunice A3, Kamenice 5*

*62500 Brno*

*Czech Republic*

*E-mail: p.simara@mail.muni.cz*

Received for publication June 29, 2017

Accepted after revision November 8, 2017

Prepublished on Liebert Instant Online November 8, 2017